universität wien

MASTERARBEIT / MASTER'S THESIS

Titel der Masterarbeit / Title of the Master's Thesis

"Molecular profiling of striated muscles from the medusa of the hydrozoan *Clytia hemisphaeria*"

verfasst von / submitted by

Lukas Rafael Kremp

angestrebter akademischer Grad / in partial fulfilment of the requirements for the degree of

Master of Science (MSc)

Wien, 2023 / Vienna 2023

Studienkennzahl lt. Studienblatt / degree programme code as it appears on the student record sheet:	UA 066 831
Studienrichtung lt. Studienblatt / degree programme as it appears on the student record sheet:	Masterstudium Zoologie
Betreut von / Supervisor:	Univ.-Prof. Dipl.-Biol. Dr. Ulrich Technau

Acknowledgements

First, I would like to thank all members of the Technau Lab and the Department of Molecular Evolution and Development for their constructive comments and the nice work environment.

I especially thank Oliver Link for his time and effort in mentoring and advising me during my time at the department and while writing this thesis. Oliver, your advice, guidance, and comments have been invaluable to me during this time.

I would like to profusely thank Ulrich Technau for giving me the possibility to perform my laboratory work in his lab, for always having an open door and open ear and for the constructive criticism during presentations and during discussions.

A very special thanks goes to the technical staff of the department, who were always able to assist me with questions.

Thank you also to Richard Latham of the Zimmer Lab, who graciously provided me with custom 3D-printed parts for the laboratory.

Table of Contents

Abstract

Striated muscles are found in most Bilateria and some basally branching animals, such as jellyfish. Although all striated muscles look similar on a morphological level, their molecular repertoire largely differs, indicating that they evolved convergently among all animals. For this thesis, a single-cell RNAseq library from a young *Clytia hemisphaerica* medusa was screened for the molecular profiles of muscles by validating muscle cluster identities via marker gene identification and cloning, *in-situ* hybridization and phalloidin staining. Furthermore, genes associated with sarcomere assembly in striated muscles of Bilateria were identified using a gene ontology (GO)-term based filtering pipeline to search for potential targets for functional studies in the future. Additionally, the onset of striation in developing medusae was determined and the feasibility for electropermeabilization in early developing medusa buds was assessed to be able to pass small molecules through cell membranes. Single cell transcriptomes of *Clytia* muscles form two clusters in the two-dimensional Uniform Manifold Approximation and Projection (UMAP) projection. These two UMAP clusters could be spatially identified as either smooth muscles of the medusa manubrium and umbrella or striated muscles located in the medusa umbrella or velum. Further we identified some genes in one of these clusters that are indeed associated with GO-terms specific to bilaterian striated muscles. We also found that medusa buds survive electroporation and molecules can be delivered into cells. These results contribute to the understanding of muscles in *Clytia hemisphaerica* and help to establish functional studies in the future.

Zusammenfassung

Gestreifte Muskeln finden sich bei den meisten Bilateria und einigen basal verzweigten Tieren, wie z. B. Quallen. Obwohl alle quergestreiften Muskeln auf morphologischer Ebene ähnlich aussehen, unterscheidet sich ihr molekulares Repertoire weitgehend, was darauf hindeutet, dass sie sich bei allen Tieren konvergent entwickelt haben. Für diese Arbeit wurde eine Einzelzell-RNAseq-Bibliothek aus einer *jungen Clytia hemisphaerica* Medusa auf die molekularen Profile der Muskeln untersucht, indem die Identitäten der Muskelcluster durch Identifizierung und Klonierung von Markergenen, *in-situ*-Hybridisierung und Phalloidin-Färbung validiert wurden. Darüber hinaus wurden Gene, die mit dem Aufbau von Sarkomeren in quergestreiften Muskeln von Bilateria assoziiert sind, mit Hilfe einer auf gene ontology (GO)-Begriffen basierenden Filterpipeline identifiziert, um nach potenziellen Zielen für zukünftige Funktionsstudien zu suchen. Darüber hinaus wurde der Beginn der Streifung in sich entwickelnden Medusen bestimmt und die Möglichkeit der Elektropermeabilisierung in sich früh entwickelnden Medusen-Knospen untersucht, um kleine Moleküle durch die Zellmembranen zu leiten. Einzelzell-Transkriptome von Clytia-Muskeln bilden zwei Cluster in der zweidimensionalen Uniform Manifold Approximation and Projection (UMAP)-Projektion. Diese beiden UMAP-Cluster konnten räumlich entweder als glatte Muskeln des Medusenmanubriums und des Medusenschirms oder als quergestreifte Muskeln im Medusenschirm oder Velum identifiziert werden. Außerdem identifizierten wir in einem dieser Cluster einige Gene, die tatsächlich mit GO-Begriffen assoziiert sind, die spezifisch für gestreifte Muskeln von Bilateralen sind. Wir fanden auch heraus, dass Medusen-Knospen die Elektroporation überleben und Moleküle in Zellen gebracht werden können. Diese Ergebnisse tragen zum Verständnis der Muskeln von Clytia hemisphaerica bei und helfen bei der Durchführung künftiger funktionaler Studien.

1 Introduction

1.1 Striated muscles among the metazoan tree of life

Muscles are a hallmark of Metazoa, allowing complex motility and movements in animals. Muscle contraction is mostly based on the interplay of aligned actin and myosin molecules (Colgren and Nichols, 2022; Sandow, 1952; Schmidt-Rhaesa, 2007). Muscle tissue is found in all animal groups except Porifera and Placozoa (Leclère and Röttinger, 2017; Musser et al., 2021; Paniagua et al., 1996). However, even though sponges lack specialized muscle cells, it has been shown that they do possess a contractile tissue called pinacoderm. This tissue contains actin, myosin, the structural striated myosin heavy chain (stMyHC) component and further proteins associated with muscles in other organisms, such as striated myosin light chain kinase (MLCK) (Colgren and Nichols, 2022). This highlights that central proteins of the muscular complex and contractile module are extremely conserved throughout animal evolution. Strikingly, striated muscles were even identified in *Euplokamis dunlapae,* a ctenophore species (Mackie et al., 1988). Interestingly, ctenophores were recently reported as being the sister group to all other animals (Schultz et al., 2023). Within the Eumetazoa, two main types of muscles depending on their ultrastructural appearance can be distinguished, called smooth and striated muscles (Fig. 1, Brunet et al, 2016). The different appearances are based on the arrangement of actomyosin filaments within the cell. In striated muscles, they are organized into sarcomeres, which are regularly arranged contractile subunits. The regular appearance comes, among others, from so-called z-discs, which represent the borders between the sarcomeres (Fig. 1, Brunet et al., 2016; Mansfield and Neumann, 2019). In addition to the actomyosin complex, further crucial proteins can be found in sarcomeres of Bilateria. These include for example the crucial protein titin, which connects myosin to the z-band, and the regulatory troponins such as Troponin C (Steinmetz et al., 2012). In contrast to striated muscles, smooth muscles are not organized in sarcomeres. In smooth muscles, no sarcomeres exist, instead, structures called dense bodies can be found, which also act as anchors for actin filaments (Fig. 1, Brunet et al., 2016). Whether the dense bodies are analogous to z-disc is thus far not known. In vertebrates, striated muscles are typically found in organs which can be voluntarily contracted, such as the skeletal muscles in humans.

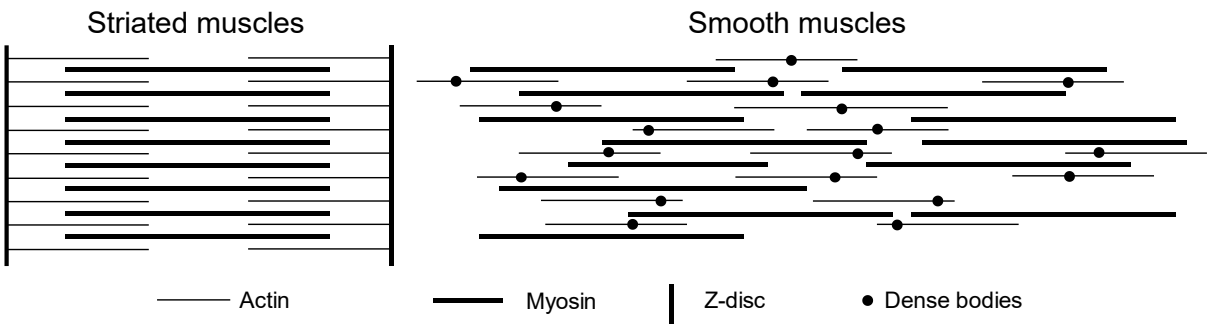

Fig. 1: Schematic representation of striated and smooth muscles. Figure based on Brunet et al. (2016).

However, some exceptions exist, as the cardiac muscle of Vertebrata also consists of striated muscle cells, yet they cannot be controlled voluntarily. Smooth muscle tissue, on the other hand, is exclusively found in organs which show involuntary contraction, e.g., the stomach or blood vessels (Haycraft, 1890). With the exception of arthropods and nematodes, smooth muscles are present in all groups of vertebrates and muscle-bearing invertebrates (Paniagua et al., 1996; Schmidt-Rhaesa, 2007). Smooth muscles are characterized by being able to provide strong contraction force over a long period of time while using little energy, whereas striated muscles are known to be able to rapidly contract (Craig and Padrón, 2004; Gabella, 1984). Striated muscles are found in most Bilateria, with few apparent losses, e.g., in flatworms. However, they are only present in a few groups of non-bilaterians, more specifically the medusa (or jelly-fish)-producing clades of Cnidaria (thus called Medusozoa), and in one species of ctenophores, *Euplokamis dunlapae* (Brunet et al., 2016; Mackie et al., 1988; Schmidt-Rhaesa, 2007). Intriguingly, while having a very similar ultrastructural appearance, the molecular machinery of striated muscles varies considerably between Cnidaria and Bilateria, but also within Bilateria between Protostomia and Deuterostomia. While muscles in all these groups contain orthologs of proteins such as actin, myosin, tropo-myosin, and calmodulin, non-Bilateria lack the regulatory troponin T, I and C proteins of the bilaterian striated muscle contractile machinery. Even more interestingly, orthologs of genes encoding for bilaterian z-disc proteins including titin are not present in cnidarians (Steinmetz et al., 2012). Recently, a study showed that paralog genes of the basic Helix-Loop-Helix transcription factor (bHLH-TF) family are involved in the formation of muscles in of the anthozoan *N. vectensis*, which are morphologically smooth (Jahnel et al., 2014, Cole et al., 2023). However, according to Brunet et al. (2016), bHLH-TF family members are not found in the core regulatory complex of ver-tebrate smooth muscles. These findings have led to the conclusion that striated

muscle tissues might have evolved through convergent evolution between Cnidaria and Bilateria but also in the Bilateria between Protostomia and Deuterostomia. Further research is being conducted on this topic, as through the positioning as sister group to all Bilateria cnidarians provide the unique opportunity to study the relationship between striated and smooth muscles in both groups and give further insights into the evolutionary relationship of these cell-types (Cole et al., 2023; Leclère and Röttinger, 2017).

1.2 *Clytia hemisphaerica* and its advantages as a model organism

Clytia hemisphaerica L. 1767 is a marine member of the hydrozoans a group within the subphylum Medusozoa. In contrast to *Hydra*, *Clytia* belongs to the colonial hydrozoans and primary polyps therefore expand through vegetative growth along a stolon which can branch and produce sprawling colonies (Fig. 2). Two specialized types of polyps are found in such a colony, called the gastrozooid (feeding polyp) and the gonozooid (reproductive polyp). Inside of the gonozooid, which is surrounded by a protective structure called theca, multiple medusa buds grow and develop along a stalk (Fig. 2). These medusa buds have a pronounced axis. At the proximal side, the bud is attached to the stalk of the gonozooid. The opposing end is termed the distal side, where the future opening of the bell as well as tentacles are located. *C. hemisphaerica* medusa buds and medusae both display tetramerous symmetry, a special form of radial symmetry in which the animal can be divided into four equal parts (Bouillon et al., 2004; Shao et al., 2020). In jellyfish forming clades, striated muscles are specifically found in the free-swimming stage and develop in the early medusa (Leclère and Röttinger, 2017). During development of the *Clytia* medusa, a third tissue next to endo- and ectoderm called the “entocodon” gives rise to smooth and striated muscles of the subumbrella (Burton, 2008). It has been shown that the entocodon also follows the tetramerous symmetry (Kraus, 2013). In *Clytia*, medusa buds are produced from specialized Gonozooids and laterally grow on a stalk located within a vessel called “Theca” (Fig. 2, Kraus, 2013). Once the small medusae develops an umbrella, they detach and are released into the surrounding water. These baby medusae can be easily distinguished from older stages by having four tentacles emerging from one tentacle bulb each, which in turn are knob-like structures located on the rim of the bell (Fig. 2, Peron et al., 2021).

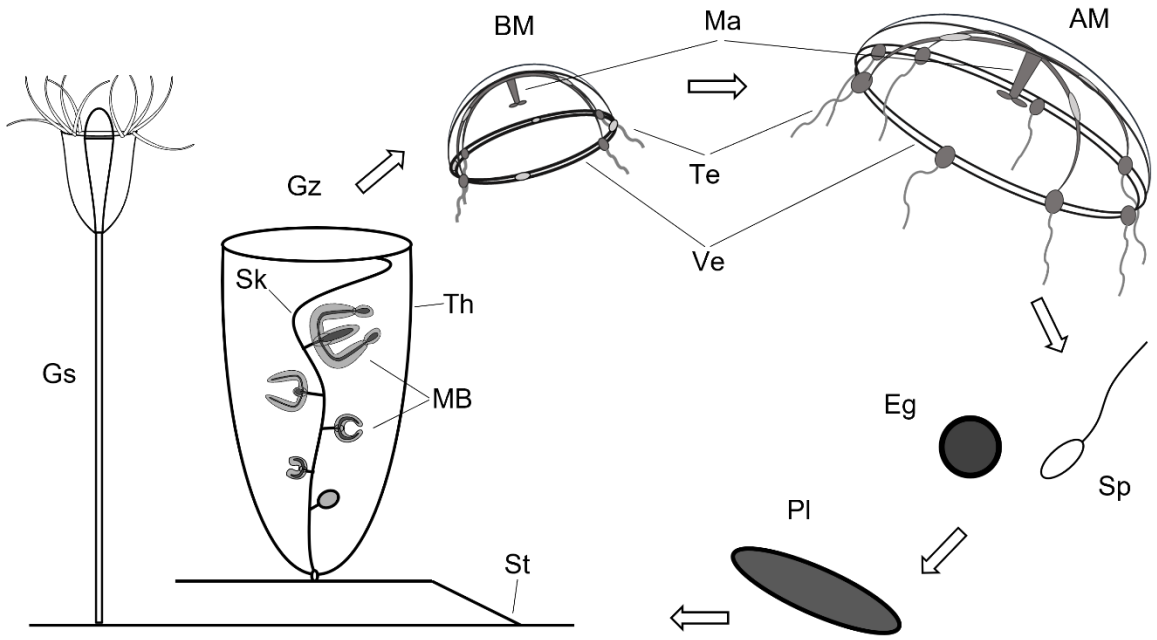

Fig. 2: Life cycle of *Clytia hemisphaerica*. Gs: gastrozooid, Gz: gonozooid, Sk: stalk, Th: theca, MB: medusa buds, St: stolon, BM: baby medusa, AM: Adult medusa, Ve: velum, Te: tentacles, Ma: Manubrium, Eg: eggs, Sp: spermatozooids, Pl: planula.

Furthermore, the freshly hatched baby medusae have a very pronounced hemispherical appearance, which will gradually flatten with increasing age (Peron et al., 2021). As the medusa grows and matures, secondary tentacles start to appear. The age of medusae can thus be assessed by the number of tentacles and tentacle bulbs. During maturation, the bell of the medusa expands in diameter, being able to reach up to 2 cm in width (Fig. 2). As the medusa matures, either male or female sexual reproductive organs develop, which are positioned along four radial canals (Peron et al., 2021). After fertilization, a free-swimming planula larva will develop. This larva will eventually settle down to the sea floor and will give rise to a new polyp colony after metamorphosing into a primary polyp (Fig. 2, Leclère et al., 2019). This primary polyp will grow into a gastrozooid and through vegetative growth along the stolon, produce a new colony with multiple gastro- and gonozooids (Fig. 2). All medusa stages can propel through the water using contractions of the concentric striated muscles spread throughout the subumbrella and the velum at the margin of the bell (Fig. 2). Medusae feed by catching prey with their tentacles containing nematocytes. Nutrients in the medusae are spread through the four radial canals extending from the base of the manubrium to the bell rim, as well as through a circular canal surrounding the umbrella rim (Peron et al., 2021). Sensory organs in medusae include statocysts, through which the animal can detect its orientation while swimming (Houliston et al., 2010).

C. hemisphaerica has many favorable traits such as all life stages being transparent, simple cultivation methods under laboratory conditions, the production of large amounts of specimens through asexual reproduction and laboratory control of the complete life cycle with polyp and medusa stages. Furthermore, the polyps' remarkable regenerative capabilities render the colony virtually immortal, as one gastrozooid with a portion of stolon, which contains multipotent i-cells, is sufficient to start an entire new colony (Carré and Carré, 2000; Lechable et al., 2020). Therefore, the species has emerged as a model organism for development and regeneration, and its use as a laboratory animal can be expected to become more widespread in the future (Houliston et al., 2010; Houliston et al., 2022; Peron et al., 2021). Leclère et al. (2019) published a genome for *C. hemisphaerica* and more recently a single-cell RNA sequencing atlas has become available (Chari et al., 2021). The transparency of all life stages of *Clytia* is advantageous for cell biological experiments as well as investigation of gene expression patterns using *in-situ*-hybridization (ISH) without the need to bleach the animal. Furthermore, its small size of all stages allows for an entire specimen to be mounted. Indeed, WMISH (whole mount *in-situ* hybridization) is extensively used on *Clytia* with the establishment of an alternative ISH protocol substituting toxic formamide with urea being first reported in this species (Sinigaglia et al., 2018). Functional approaches have been described in the past using microinjections of morpholinos and mRNAs (Amiel et al., 2009; Momose and Houliston, 2007), with knockout studies utilizing CRISPR/Cas9 emerging in more recent years (Momose et al., 2018; Quiroga Artigas et al., 2018; Quiroga Artigas et al., 2020). Transgenesis is not yet as well established as in other cnidarian model organisms such as *Nematostella vectensis*, yet it has been shown that the generation of stable transgenic lines is, in principle, feasible (Weissbourd et al., 2021). However, while early embryonic stages are accessible for gene manipulation methods, functional studies in Clytia medusae have yet to be established.

1.3 Aims of the project

For this master thesis, I address the following questions:

Are we able to identify and describe molecular profiles of muscles from young Clytia *medusae?*

The localization of muscles was determined by use of phalloidin stainings. This spatial information was used to look for an overlap with marker gene expression patterns gained from WMISH (while mount *in-situ* hybridizations). Therefore, marker genes were selected from differentially expressed genes of the expected muscle profiles. Furthermore, molecular fingerprints of muscles were dissected into two different categories such as structural genes (e.g., genes necessary for the contractile core complex, membrane transporters and receptor genes) and transcription factors.

Do striated muscles from Clytia *medusae share molecular components involved in sarcomere assembly of Bilateria?*

Additionally, striated muscles were subjected to gene ontology (GO) filtering associated with GO terms of bilaterian striated muscles. This process was meant to identify potential targets for functional studies.

Is electroporation a potential tool to guide small molecules through cell membranes in developing medusae in C. hemisphaerica?

For a deeper understanding of the relationship of striated muscles from different animal phyla studies investigating gene function must be conducted. Here, an assay which includes survivability of early medusa buds after electroporation as well as the delivery of small molecules into cells was performed. This stage was chosen as it was deemed desirable to analyze the function of specific genes associated with sarcomere assembly in early medusa development. Thus, the onset of striation during medusa development in medusa buds was followed by phalloidin stainings.

Does the subumbrella expand by uniform cell division?

As a side project, it was investigated whether the subumbrella might expand during medusa growth by allometric growth through 5-Ethynyl-2'-deoxyuridine (EdU) staining.

2 Materials & Methods

2.1 *Clytia hemisphaerica* animal culture

Fig. 3: Culture system of *Clytia hemisphaerica*. **A:** Cylindrical tanks with vertical microscope slides as base for the polyp colonies. **B:** Kreisel-tanks for all medusae stages.

C. hemisphaerica polyp colonies and medusae were kept in the dark at 20°C in 38‰ artificial sea water (ASW). Polyp and medusae colonies were kept in separate tanks. Both stages were further separated by sex. Polyps were raised in cylindrical tanks, in which microscope slides were inserted vertically on a 3D-printed plug-in frame (Fig. 3A). The polyp colonies were growing along these slides. As soon as young medusae were budding off of the colony and began to swim freely in the ASW, they were collected with a glass Pasteur pipette and transferred to a Kreisel-tank (3 L Kreisel – Zuchtaquarium, Jellyfish Farm, Germany) where they continued to grow (Fig. 3B). The water circulation in the tanks was supported by an attached air pump. Both polyps and medusae were fed daily on weekdays *ad libitum* with freshly hatched *Artemia salina* nauplii. ASW for the polyp colonies was exchanged against fresh ASW weekly,

whereas the medium for medusae was changed every two weeks. Furthermore, the surface of the microscope slides was screened at least once a week and debris such as dead polyps, algae etc. was scraped off with a toothpick.

Polyp colony propagation was based on a previously described study (Fig. 4, Lechable et al., 2020). Gastrozooids were cut out from the colony leaving a bit of stolon attached to the polyp using a microscalpel (e.g., FEATHER No. 745, Cat. No. 08-924-24, fisher scientific, USA) and placing them on a previously washed microscope slide lying horizontally in a petri dish containing enough ASW to cover the slide. The gastrozooids were then fed with *Artemia* larvae and left undisturbed overnight so that they can attach to the surface. The following day, the slides were transferred to the polyp culture tanks and continued to grow into colonies producing both kinds of polyps and thus producing new medusae.

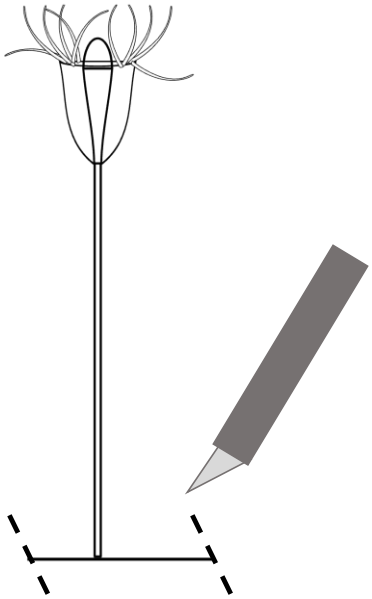

Fig. 4: Scheme representing the propagation of the colony, by cutting out a gastrozooid out (on the dashed lines) but leaving a bit of stolon still attached.

2.2 Collection & fixation of animals

Gonozooids were collected by cutting off the lid of the polyp with very fine (tip diameter 0.075 mm) micro scissors (e.g., Cat. No. 15003-08, F.S.T., Canada). The scissors were then applied to the base of the polyp, as close as possible to the stolon, and were used as a pair of fine tweezers to gently push the medusa buds and the stalk out of the theca. The stalk containing the buds was then collected with a Pasteur pipette and transferred to a 1.5 ml tube containing ASW. Medusae were placed directly into tubes containing ASW. All specimens were then washed once by exchanging the ASW against 38‰ filter sterile ASW (FSASW) and relaxed by keeping the tubes at 4°C until no more contraction of the bell could be observed. Unless stated otherwise, animals were fixed by adding dropwise an equal volume of pre-chilled 8% paraformaldehyde (PFA) to obtain a final concentration of 4% PFA and placed on an overhead rotator at 4°C for up to 24 h. Afterwards, the fixative was washed out at least thrice with 0.1% PTw (Phosphate-buffered saline, PBS, containing 0.1% Tween-20). The washed specimens were then either directly used for experiments or stored for later use by keeping them in >96% Methanol (MeOH) at -20°C.

2.3 Phalloidin staining

Freshly fixed animals were washed three times with 0.1% PTw and permeabilized for 5 mins with 0.5% PBT. They were washed with PBS and blocked for 2 mins with 3% w/v bovine-serum albumin (Cat. No. A7906, Sigma-Aldrich, USA). For filamentous actin staining, either phalloidin Alexa Fluor 488 or 568 (Cat. No. A12379 & A12380, respectively, both Invitrogen, USA) in a concentration of 1:50 in PBS was added and left on an overhead rotator at 4°C overnight. The phalloidin was washed out thrice with 0.1% PTw, with the last wash being at least 30 mins long. The samples were then infiltrated with VECTASHIELD antifade mounting medium containing 4′,6-diamidino-2-phenylindole (DAPI, Cat. No. H-1200-10, Vector Laboratories, USA), mounted on microscope slides and imaged.

2.4 Identification and cloning of marker genes

Pre-analysis of scRNAseq data was performed by Oliver Link prior to this study, resulting in the identification of two putative muscle clusters. Molecular profiles of these clusters were screened for potential marker genes. Therefore, the top 10 differentially expressed genes were visualized using dot plots from the Seurat package (Hao et al., 2022) in R v4.2.2 (R Core Team, 2022). GO-filtering was done using dplyr (Wickham et al., 2023). The code used provided by Oliver Link (personal communication) can be found in supplementary section S5 with a list of GO-terms used for filtering also attached (supplementary Table S19). These terms were chosen as they are specific to bilaterian sarcomere assembly. Potential marker genes were selected for cloning if their *in-silico* expression pattern was mostly confined to the putative muscle clusters. Afterwards, primers for these genes were designed using Primer3 (primer3.ut.ee/, Koressaar and Remm, 2007; Koressaar et al., 2018; Untergasser et al., 2012) considering the following parameters: primer length18-23 nt, T_m 54°C-62°C, T_m difference between forward and reverse primer less than 2°C, and final product size between 700 and 1500 bp. Binding specificity of the primers was then checked in order to minimize the risk of the primers accidentally binding to different genes. All primers were ordered from Microsynth (www.microsynth.com). More primer information can be found in the supplemental information section S1. The marker genes were amplified by polymerase chain reaction (PCR) with the gene-specific primers using a complementary DNA (cDNA) template. The cDNA template was generated by reverse-transcription of RNA

extracted from different medusa stages using phenol-chloroform RNA extraction. For this PCR, Q5 High Fidelity DNA polymerase (Cat. No. M0491S, New England Biolabs, USA) creating a blunt-end product was utilized. Afterwards, the PCR product was gel-extracted using the Monarch DNA Gel extraction Kit (Cat. No. T1020S/L, New England Biolabs, USA) according to the manufacturer's protocol. The extracted product was then ligated to the pJET1.2/blunt vector following the instructions provided by the manufacturer, with the ligation time prolonged to 10 mins. All chemicals for the ligation were taken from the CloneJET PCR cloning kit (Cat. No. K1231, Thermo Scientific, USA). 3 µl of the ligation mix were then added to 50 µl of competent 5-alpha *Escherichia coli* bacterial cells (Cat. No. C2987, New England Biolabs, USA). After gently mixing by flicking and incubating the mixture on ice for 10 mins, the cells were transformed by heat shock at 42°C for 45 sec, subsequently placing them back on ice for at least 2 mins. The cell suspension was then transferred to pre-heated agar plates containing ampicillin as a selection agent against untransformed cells and incubated at 37°C overnight. The following day, clearly identifiable single clones were picked off the plates with clean pipette tips and transferred to a new plate and into PCR tubes containing milli-Q-purified H_2O. The cell-water mix was then used for an insert-PCR, checking whether the cell colonies contained an insert of the desired size. The new plate was placed back into the 37°C-incubator to allow the transferred clones to regrow to a sufficient size, after which they were placed into 5 ml liquid broth medium containing ampicillin, which was again incubated overnight at 37°C with agitation by shaking. From these liquid cultures, the vectors with the insert were extracted from the *E. coli*-cells using the innuPREP Plasmid Mini Kit 2.0 (Cat. No. 845-KS-5041250, IST Innuscreen, Germany) following the instructions provided by the manufacturer. The purified vectors were sequenced, performed by Microsynth, to verify that they contain the correct insert and to check the orientation of the insert. As the pJET1.2/blunt vector only contains one T7 promotor, but lacks a SP6 promotor, a further PCR using a primer attaching a SP6 promotor to the product was conducted. This process also linearized the insert. The PCR product was purified by sodium acetate precipitation and then used for RNA-probe synthesis. Probe synthesis was achieved by using either the HiScribe T7 or HiScribe SP6 RNA Synthesis Kits (Cat. No. E2040S & E2070S, respectively, both New England Biolabs, USA), depending on the orientation of the insert to obtain an antisense probe. Instead of the NTPs provided by the kits, a NTP mix containing digoxigenin (DIG)-labelled UTP (Cat. No. 11277073910, Roche, Switzerland)

was used. Furthermore, RNAseOUT ribonuclease inhibitor (Cat. No. 10777019, Invitrogen, USA) was included in the transcription mix at a final concentration of 2 U/µl. The transcription was performed overnight at 37°C, followed by DNA digestion for 20 mins at 37°C using RNAse-free DNAse I (Cat. No. M3030, New England Biolabs, USA). The probe was precipitated for at least 2 h at -20°C by adding an equal volume of both LiCl and RNAse-free H_2O, after which it was purified by centrifugation and then diluted to a final concentration of 50 ng/µl with deionized formamide (Cat. No. P040.1, Carl Roth, Germany), finally being stored at -20°C for later use.

2.5 Whole mount *in situ* hybridization (WMISH)

For a detailed composition of buffers and a detailed WMISH protocol, please refer to supplementary sections S2 and S3, respectively. In brief, animals stored in MeOH were transferred to >96% ethanol (EtOH), followed by stepwise rehydration with 0.1% PTw. They were then pre-hybridized in a urea-containing buffer (Sinigaglia et al., 2018), followed by hybridization with the DIG-labeled probe at 57°C overnight. The following day, the samples were gradually washed into sodium-salt-citrate buffer, subsequently washed into 0.1% PTw and permeabilized with 0.5% PBT (PBS containing 0.5% Triton-X 100, Cat. No. T8787, Sigma-Aldrich, USA). After blocking the specimens, they were incubated overnight in the presence of an anti-DIG antibody conjugated with alkaline phosphatase (AP, Cat. No. 11093274910, Roche, Switzerland) at 4°C. The antibody was washed out at least eight times with 0.2% PBT, after which the animals were incubated thrice in AP buffer, followed by adding the staining solution. As soon as the animals were stained, the staining solution was removed, the specimens were washed once with 0.1% PTw and left in >96% EtOH 2 h to overnight at 4°C. For mounting and imaging, EtOH was removed, and the samples were infiltrated with >86% glycerol and then placed on microscope slides. WMISH stainings were performed at least three times with a minimum of three specimens per repetition.

2.6 Electroporation procedure

For electroporation, *C. hemisphaerica* gonozooids were harvested and washed once with FSASW. The polyps were then suspended in FSASW containing 15% Ficoll. For tracing experiments, 2% of dextran conjugated with AlexaFluor 568 was then added to the solution. Alternatively, 1 µg/ml of capped mCherry RNA mimicking mRNA

generated with either the T7 or SP6 mMESSAGE mMACHINE kit (Cat. No. AM1344 or AM1340, respectively, both Invitrogen, USA) was added to the mix. 200 µl of the solution containing at least ten gonozooids per electroporation were transferred to an electroporation cuvette. The electroporation was performed using the Gene Pulser Xcell system (Cat. No. 1652660, Bio-Rad, USA) providing a single 50 V square wave pulse for 25 ms. These settings are known to be viable for *C. hemisphaerica* larvae (Masuda-Ozawa et al., 2022). After electroporation, the polyps were transferred to either a small petri dish or a well plate containing >5 ml fresh FSASW, which was exchanged daily. The animals were kept in the dark on a rocking platform to keep the medium in movement. They were screened each day for medusa formation, survival and for a color signal using a fluorescent stereo microscope. Survival was assessed as medusae being able to swim and feed. Feeding was done every day with approximately one *Artemia* nauplii per living medusa in the medium.

2.7 5-Ethynyl-2'-deoxyuridine (EdU) staining

Freshly collected animals were placed in FSASW containing 30 µM EdU from the Click-iT EdU Cell Proliferation Kit (Cat. No. C10340, Invitrogen, USA) for 30 mins at room temperature. During the last 5 mins of EdU labelling, they were relaxed by placing them at 4°C. The EdU solution was removed, and the specimens were fixed for 2 h at 4°C using an overhead rotator with a 4% PFA solution in 0.1% PTw. Afterwards, the fixative was washed out thrice using 0.1% PTw for 5 mins each step. The tissue was permeabilized using a 30 min incubation with 0.5% PBT. Then, the specimens were incubated for 2 h in the dark at room temperature in EdU detection buffer (for composition, refer to supplementary Table S10) with agitation through a rocking platform. The samples were washed three times with 0.1% PTw, followed by nucleotide staining using DAPI 1:1000 in 0.1% PTw for 30 mins. After the DAPI solution was washed out three times using 0.1% PTw, the specimens were infiltrated with VECTASHIELD mounting medium containing DAPI and left overnight at 4°C, after which they were mounted on microscope slides and imaged.

2.8 Imaging methods

Overview phalloidin stainings were imaged with an Eclipse Ni microscope with a DS-Qi2 camera (both Nikon, Japan). Detail phalloidin and all EdU images were taken with

a confocal laser scanning microscope model SP8 (Leica Microsystems, Germany) from the Core Facility for Cell Imaging & Ultrastructure Research (CIUS) of the University of Vienna. Monochromatic phalloidin and EdU images were adjusted for brightness and contrast using the “Auto” option within Fiji 1.54e (Schindelin et al., 2012; Schneider et al., 2012). WMISH images were taken using an Eclipse 80i microscope attached to a DS-Fi1 digital camera (both Nikon). All images for electroporation (bright-field and fluorescent) were captured with a stereo microscope (SMZ18, Nikon) using either a DS-Fi1 (Nikon) or MikroCam II 20MP camera (Bresser, Germany) with the same exposure settings for every treatment. Brightness and contrast of WMISH and electroporation images were adjusted manually using Fiji.

3 Results

3.1 Localization of striated muscles and cluster validation

3.1.1 Striated muscles are located in the subumbrella and velum of *C. hemisphaerica* medusae

F-actin stains with Phalloidin were performed to locate the striated muscles in the medusae of *C. hemisphaerica*. In freshly hatched baby medusae, which can be identified by having four tentacles and tentacle bulbs, striated muscles are distributed in the entire subumbrella (Fig. 5A-F), except for a small space on the proximal side, where the manubrium protrudes (Fig. 5C, F). Striated muscle fibers are orientated circumferentially along the subumbrella (Fig. 5D, E). Smooth muscle fibers are orientated radially, i.e., orthogonally to striated muscle fibers, so that a net-like appearance persists throughout the entire subumbrella (Fig. 5B). The smooth muscles extend towards the base of the manubrium; hence, this area is only covered by smooth fibers (Fig. 5C, F). The distally located velum forms a ring around the bell opening. It is made up entirely of striated-type musculature and appears denser than the subumbrellar musculature (Fig. 5D, E). As the medusa grows, the diameter of the bell increases at least six-fold (Fig. 5G). The age of the medusa can be assessed by an increase in the number of tentacles and tentacle bulbs, and the emergence of the gonads along the radial canals indicates maturation (Fig. 5G). During medusa aging, changes in the distribution of striated muscles can be observed.

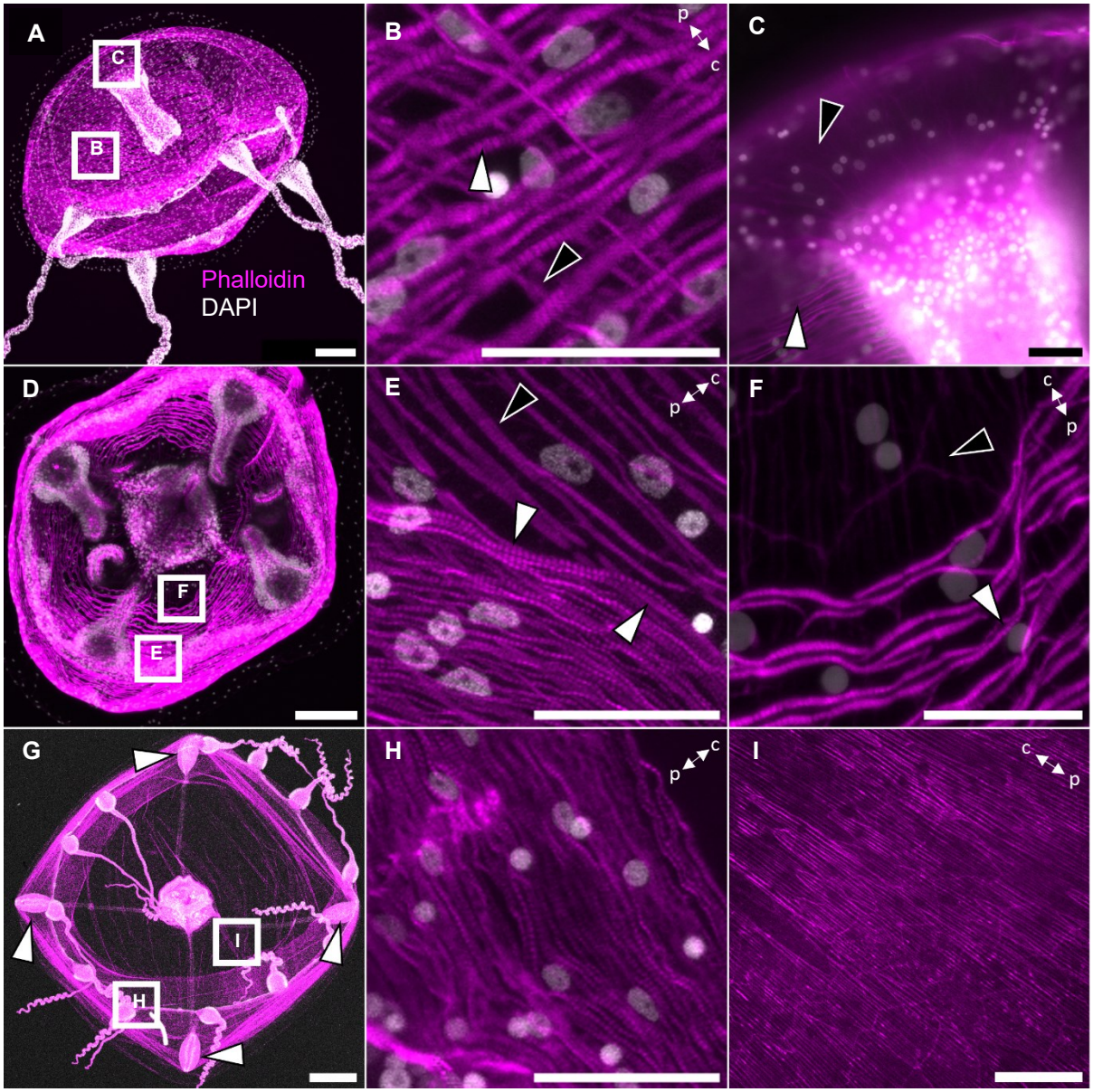

Fig. 5: Localization of striated muscles in *C. hemisphaerica* medusa. **A:** Lateral view of a juvenile medusa, identified by having four tentacle bulbs. Muscle fibers can be seen distributed throughout the entire bell. **B:** Detailed view of a segment of the bell and subumbrella. Here, the arrangement of smooth (black arrowhead) and striated (white arrowhead) muscle fibers in a net- or grid-like shape can be seen, with both types of muscles orientated orthogonally to each other. **C:** Lateral view of the proximal end of the medusa, where the manubrium extends from the bell. At this location, no striated muscles (white arrowhead) can be seen, only the smooth muscles (black arrowhead) running along the proximal-distal axis are present in this region. **D:** Juvenile medusa, oral view. This view further highlights that striated muscles (**F**, white arrowhead; black arrowhead: smooth muscles) do not reach towards the base of the manubrium. Furthermore, the different appearance of subumbrellar muscular tissue (**E**, black arrowhead) and velum (**E**, white arrowhead) becomes apparent. The velar tissue is much denser than the muscle fibers of the subumbrella. **G:** Oral view of a mature adult medusa. Here, 12 tentacles and tentacle bulbs, and four gonads can be seen in the animal, indicating maturation. **H:** Detail view over the appearance of the velum in an adult medusa. It follows the same dense arrangement as seen in a juvenile animal (**E**). **I:** Detail section of the subumbrellar tissue, showing that in adult medusae, the subumbrella is largely populated by only smooth muscles, with an apparent loss of striated muscles. Arrow shows the orientation from center (c) to periphery (p). Scale bars: 500 µm (**G**), 100 µm (**A**, **D**), 25 µm (**B**, **C**, **E**, **F**, **H**, **I**). Note that image **I** only shows the phalloidin channel and has the DAPI channel omitted, to provide a clearer view over the absence of striation in the subumbrella.

The area at the base of the manubrium at the proximal end of the subumbrella, which is void of striated muscles, broadens, and expands (Fig. 5G, I). Thus, striation in older animals is not distributed throughout the entire bell anymore but restricted more at the periphery end of the bell. The appearance of the velum, however, does not seem to change (Fig. 5H). It forms a thin piece of tissue along the bell rim densely filled with striated muscle fibers (Fig. 5E, H).

3.1.2 Muscles form clusters in the scRNAseq dataset

Single-cell RNA sequencing (scRNAseq) was performed by Oliver Link (unpublished data) on female juvenile *C. hemisphaerica* medusae. The obtained library contained roughly 9000 cells, of which their transcriptome was clustered into 16 distinct clusters (Fig. 6). The identity of these clusters was investigated by conducting a differential gene expression analysis performed beforehand by Oliver Link (unpublished), with annotation of the transcripts being based on best BLAST (Basic Local Alignment Search Tool) hits. Furthermore, the top-enriched genes in every cluster in our dataset were compared to a set of marker genes from a previously published and partly annotated scRNAseq library (Chari et al., 2021). Through this process, two clusters in our dataset were identified as containing muscles, termed muscle.1 and muscle.2. However, while Chari et al. (2021) report that one cluster in their data contains the transcripts of the striated muscles of the subumbrella and one the striated muscles of the velum, this difference was not found in our dataset. The marker genes of both of their striated muscle clusters were found to be in both of our muscle clusters, with no distinction between velum and subumbrella to be found (supplementary Fig. S1A, B). Additionally, the differentially expressed genes in our clusters were filtered for their gene ontology (GO) terms using GO-terms associated with vertebrate striated muscles (Fig. 7). This revealed that the two putative muscle clusters contain more transcripts associated with a myosin complex than other clusters, enhancing the identity of these two clusters as being muscle-specific (Fig. 7A). Overall, more than 92% (489/527) of all transcripts identified in the GO-filtering were associated with ATP-binding, protein binding, and calcium-ion binding (Fig. 7B). The other 38 transcripts were associated with GO-terms such as actin filament binding (20), myosin complex (10), actomyosin structure organization (5) and focal adhesion, tropomyosin binding and pointed-end actin filament capping (1 each, Fig. 7B).

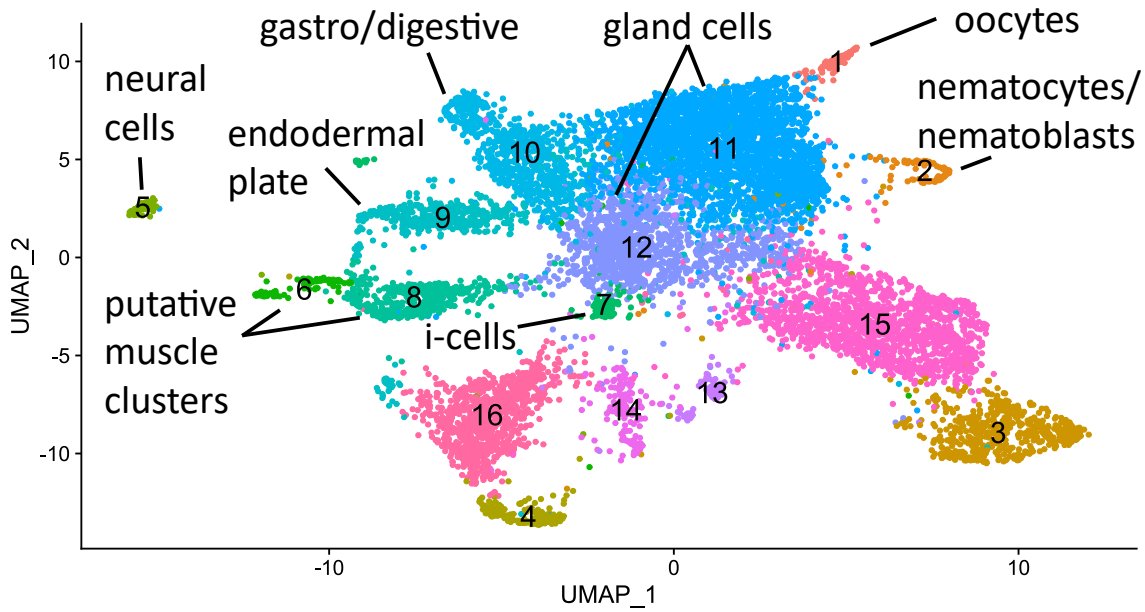

Fig. 6: Uniform Manifold Approximation and Projection (UMAP) of the clusters in our dataset, revealing 16 distinct clusters. Through comparison with a reference dataset and a differential gene analysis done by Oliver Link, clusters 6 and 8 were putatively identified to contain muscles; these clusters will be referred to as muscle.1 and muscle.2 for the remainder of this study, respectively. The names of the other clusters are based on a comparison of the marker genes the reference dataset (Chari et al., 2021) with our clusters. Clusters 3, 4 and 13 – 16 could not be verified through this comparison with the reference dataset.

Fig. 7 (following page): Results of the GO-filtering of differentially expressed genes in our dataset, revealing that ten GO-terms associated with bilaterian sarcomere assembly were found. These genes are distributed in all clusters except cluster 11 (identified as gland cells). **A**: Proportion of genes associated with muscle-GO-terms per cluster. This plot shows how the specific muscle-GO-terms are distributed among the different clusters as proportions. Note that of the 16 clusters initially identified, only 15 are represented in the GO-filtering, as cluster 11 did not contain any genes associated with bilaterian sarcomere assembly. **B**: Absolut distribution of the GO-terms. Most genes are associated with protein binding, ATP binding and calcium-ion binding.

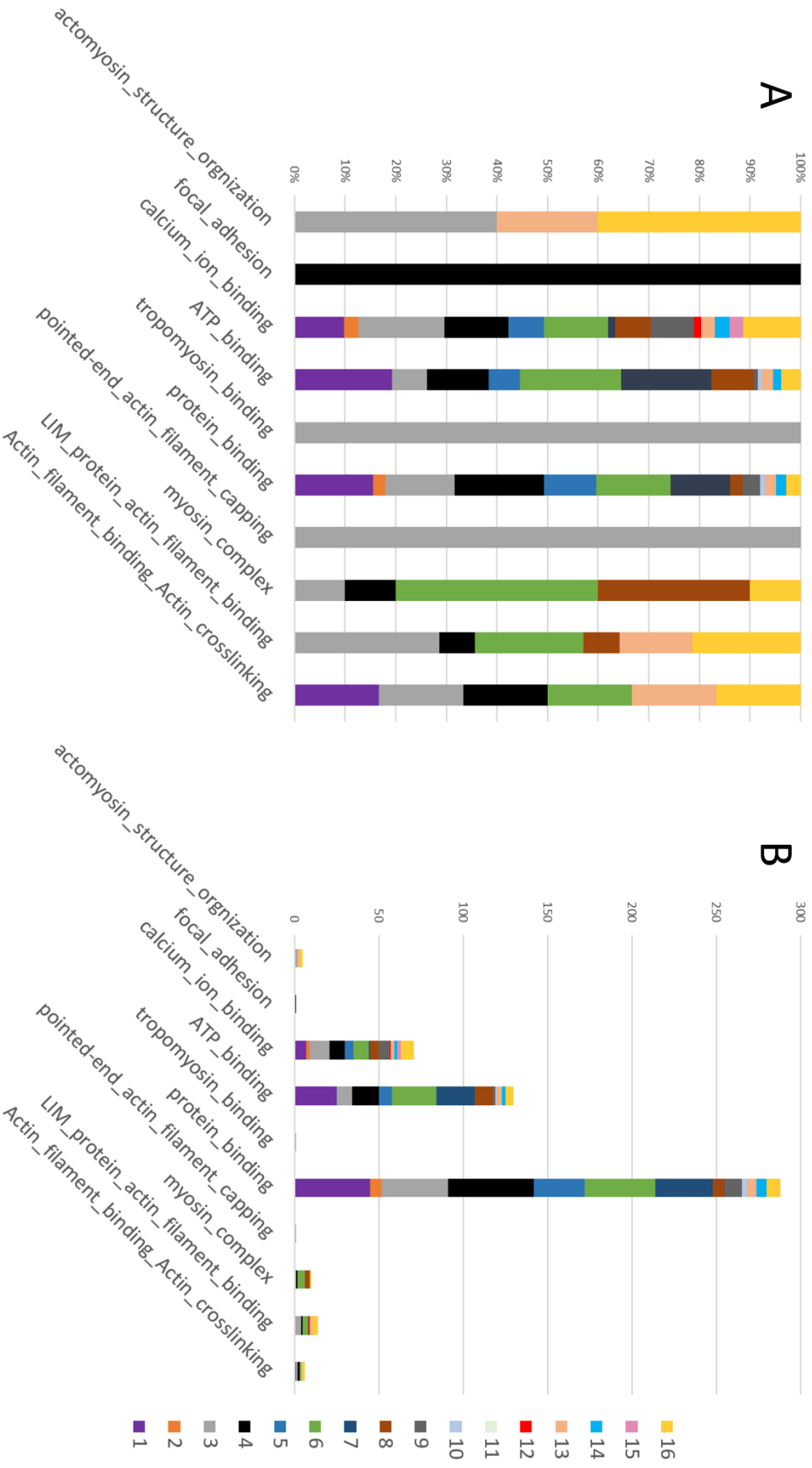
A
actomyosin_structure_orgnization
focal_adhesion
calcium_ion_binding
ATP_binding
tropomyosin_binding
protein_binding
pointed-end_actin_filament_capping
myosin_complex
LIM_protein_actin_filament_binding
Actin_filament_binding_Actin_crosslinking
0%
10%
20%
30%
40%
50%
60%
70%
80%
90%
100%
B
0
50
100
150
200
250
300
1
2
3
4
5
6
7
8
9
10
11
12
13
14
15
16

3.1.3 WMISH data validates the striated muscle cluster identity

To validate the identity of the putative muscle clusters, cluster-specific probes for WMISH stainings were generated and their staining patterns then compared to the medusae phalloidin stainings. However, most of the investigated genes were expressed *in-silico* in both clusters, and only a few were found in cluster muscle.1 only. No gene was found expressed exclusively in cluster muscle.2. Four muscle cluster specific probes could be successfully generated, i.e., the expected fragment was contained within the cloning vector. The probe sequences were preliminarily annotated as being an ankyrin repeat, ef-hand domain, and twice as myosin domains, respectively. For the remainder of this study, they will be referred to as *myotrophin-like* (*MTPN-like*), *myosin light chain-like* (*MLC-like*), and *myosin heavy chain, striated muscle-like 1* & *2* (*stMyHC-like 1* & *2*), respectively (Fig. 8).

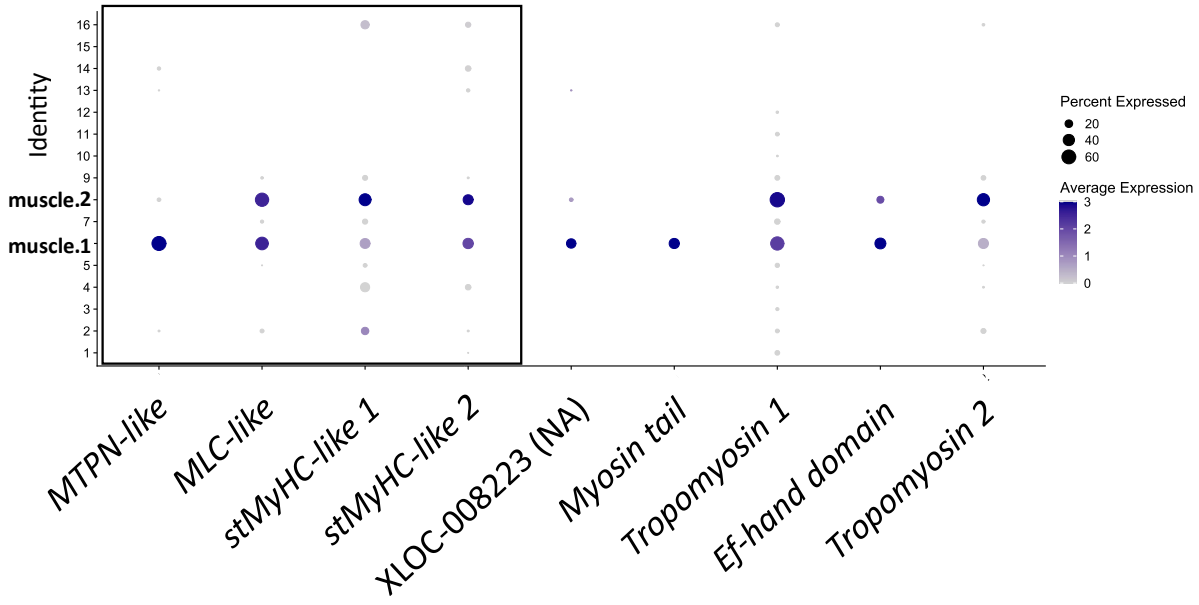

Fig. 8: Expression patterns of the four generated WMISH probes (black box) and further potential marker genes, visualized by dot plots. *Myosin light chain* (*MLC*)*-like* and *myosin heavy chain, striated muscle* (*stMyHC*)*-like 2* show a strong expression pattern in both identified muscle clusters, while *myotrophin* (*MTPN*)*-like* is only expressed in cluster muscle.1. *stMyHC-like 1* is strongly expressed in cluster muscle.2, with little expression in muscle.1, being the only successfully generated probe with such an expression pattern.

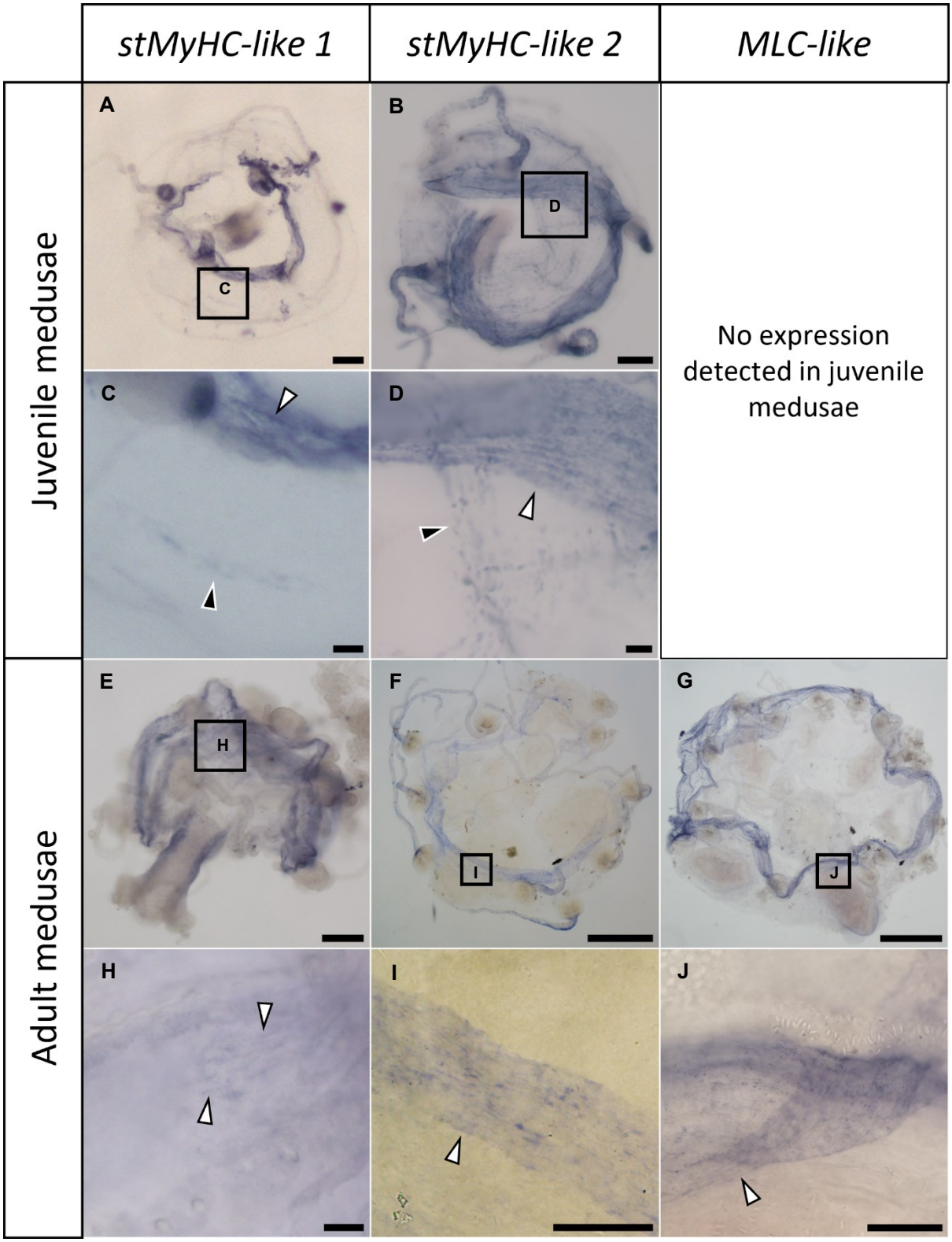
stMyHC-like 1
stMyHC-like 2
MLC-like
Juvenile medusae
Adult medusae
A
B
C
D
No expression detected in juvenile medusae
C
D
E
F
G
H
I
J
H
I
J

Fig. 9: Expression patterns of muscle cluster specific genes in juvenile and adult medusae. **A**: Oral view of *stMyHC-like 1* expression in juvenile medusae. The gene is in the velum (**C**, white arrowhead) with some expression also scattered throughout the subumbrella (**C**, black arrowhead). **B**: Oral view of *stMyHC-like 2* expression in a juvenile medusa. Expression is very pronounced in the velum (**D**, white arrowhead) and subumbrella (**D**, black arrowhead). However, the expression in the subumbrella does not extend throughout the entire bell but leaves a small space at the base of the manubrium. Furthermore, gene expression is only detected circumferential. Note that in this specimen, the velum has accidentally been ruptured during mounting. **E**: Lateral view of an adult (mature) medusa, showing *stMyHC-like 1* expression. The gene expression pattern is confined to the velum, where it follows the circumferential pattern running along the distal opening of the bell (**H**, white arrowheads). **F** and **G**: Oral views of adult medusae showing *stMyHC-like 2* and *MLC-like* gene expression, respectively. In this life stage, the expression patterns of these two genes are very similar, both genes are found in the velum forming circumferential bands (**I** and **J**, white arrowheads) but are not expressed in the subumbrella. Some expression of *stMyHC-like 2* can be found in the tentacle bulbs, whereas *MLC-like* gene expression is only found in the velum. Scale bars: 500 µm (**F**, **G**), 100 µm (**E**), 50 µm (**A**, **B**, **I**, **J**), 10 µm (**C**, **D**, **H**)

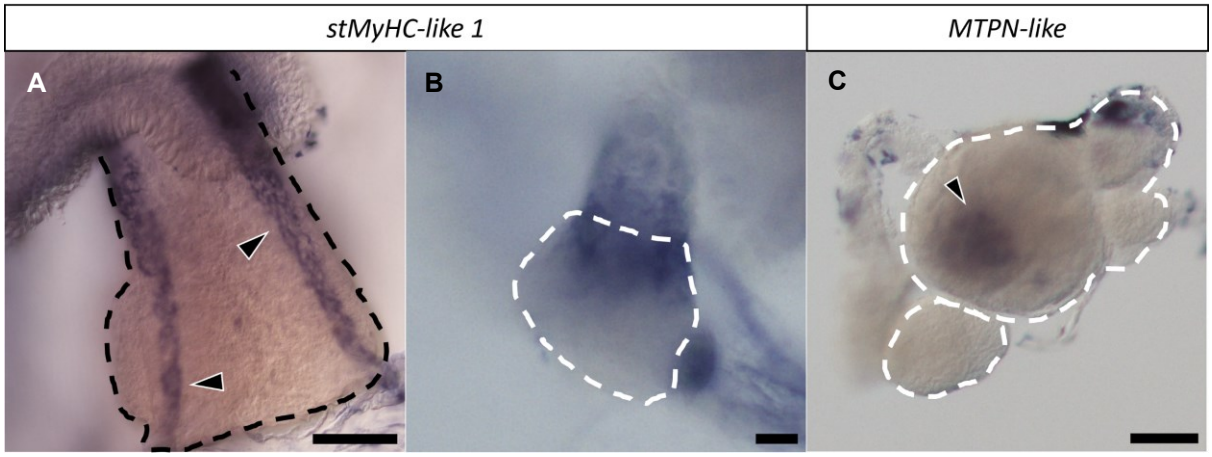

Fig. 10: Detail images of non-muscular gene expression. **A**: Lateral view of a medusa manubrium (black outline). *stMyHC-like 1* expression can be seen as four streaks located in the corners of the manubrium (black arrowheads). **B**: *stMyHC-like 1* expression in tentacle bulbs of a medusa (white outline) can be found at the distal side of the bulbs, at the side where tentacles grow out of the bulb. **C**: *MTPN-like* expression (black arrowhead) is found only at the location of the manubrium during medusa bud (white outline) development. Scale bars: 50 µm (**A**, **C**), 10 µm (**B**)

Three out of the four generated probes showed highly specific WMISH patterns in different *C. hemisphaerica* medusa stages. At all stages, gene expression of *stMyHC-like 1* and *stMyHC-like 2* can be found in the velum, while *MLC-like* is only found in adult medusae in the velum (Fig. 9C, D, H-J). The expression pattern appears as elongated fibers or streaks in the circumferential direction around the opening of the umbrella, closely resembling the appearance of the fibers visualized by phalloidin staining. The expression also shows the same dense appearance as seen in the phalloidin staining. In adult and juvenile medusae, *stMyHC-like 1* and *stMyHC-like 2* expression can be further found at the tip of the tentacle bulbs, where the tentacles grow out (Fig. 9A, B, E, F; Fig. 10B; supplementary Fig. S3D, E). These two genes are also expressed to some extent along the sides of the manubrium, where four streaks of

expression running from the tip to the base of the manubrium can be found in juvenile and sub-adult medusae (Fig. 10A; supplementary Fig. S3A, B). Staining in the manubrium or tentacle bulbs was not found for *MLC-like* (supplementary Fig. S3C, F). *stMyHC-like 2* expression can be found in the subumbrella of juvenile medusae. Here, the expression follows the same pattern as the phalloidin staining. It is not found in the entire subumbrella, as the area around the manubrium is void of gene expression (Fig. 9B, D). Furthermore, no net-like appearance is visible, with expression only visible circumferentially around the bell of the medusa. Expression in the subumbrella is also less dense than in the velum, which correlates with the observed phalloidin staining pattern (Fig. 9B, D). The expression pattern of *stMyHC-like 1* in juvenile medusae, however, is slightly different (Fig. 9A, C). While gene expression was detected in the velum, less gene expression could be detected in the subumbrella of the animals, with only patches visible in some areas. These patches, although appearing faint compared to the intensity of the velar staining, still followed the circumferential orientation of the subumbrella (Fig. 9A, C). While *stMyHC-like 1* and *stMyHC-like 2* mRNA was detected in the tentacle bulbs and the manubrium, no such staining pattern was observable in samples stained for *MLC-like*. Even after prolonged staining times, expression was confined to the area of the velum at the base of the umbrella (Fig. 9G, J). Although according to the scRNAseq-data *MTPN-like* is strongly expressed in the muscle.1 cluster, no expression of this gene was found in the umbrella or velum medusae of any age. This probe was only found to stain parts of the manubrium transiently during medusa development (Fig. 10C, supplementary Fig. S4A, B). Overall, these results indicate that cluster muscle.2 appears to very likely contain striated muscles of the velum and possibly also subumbrella while cluster muscle.1 contains smooth muscles of the manubrium.

3.1.4 The molecular profile of the putative muscle clusters

After validation of the muscle cluster identity, the molecular muscle profile of these striated muscle cell subpopulations of juvenile medusae was investigated. Both identified striated muscle clusters contain multiple genes annotated as being closely associated with muscles and muscular function (Fig. 11). These include, for example, tropomyosin, myosin and calponin. Overall, of the 15 muscle genes found in cluster muscle.2, 11 (73%) are also found in cluster muscle.1.

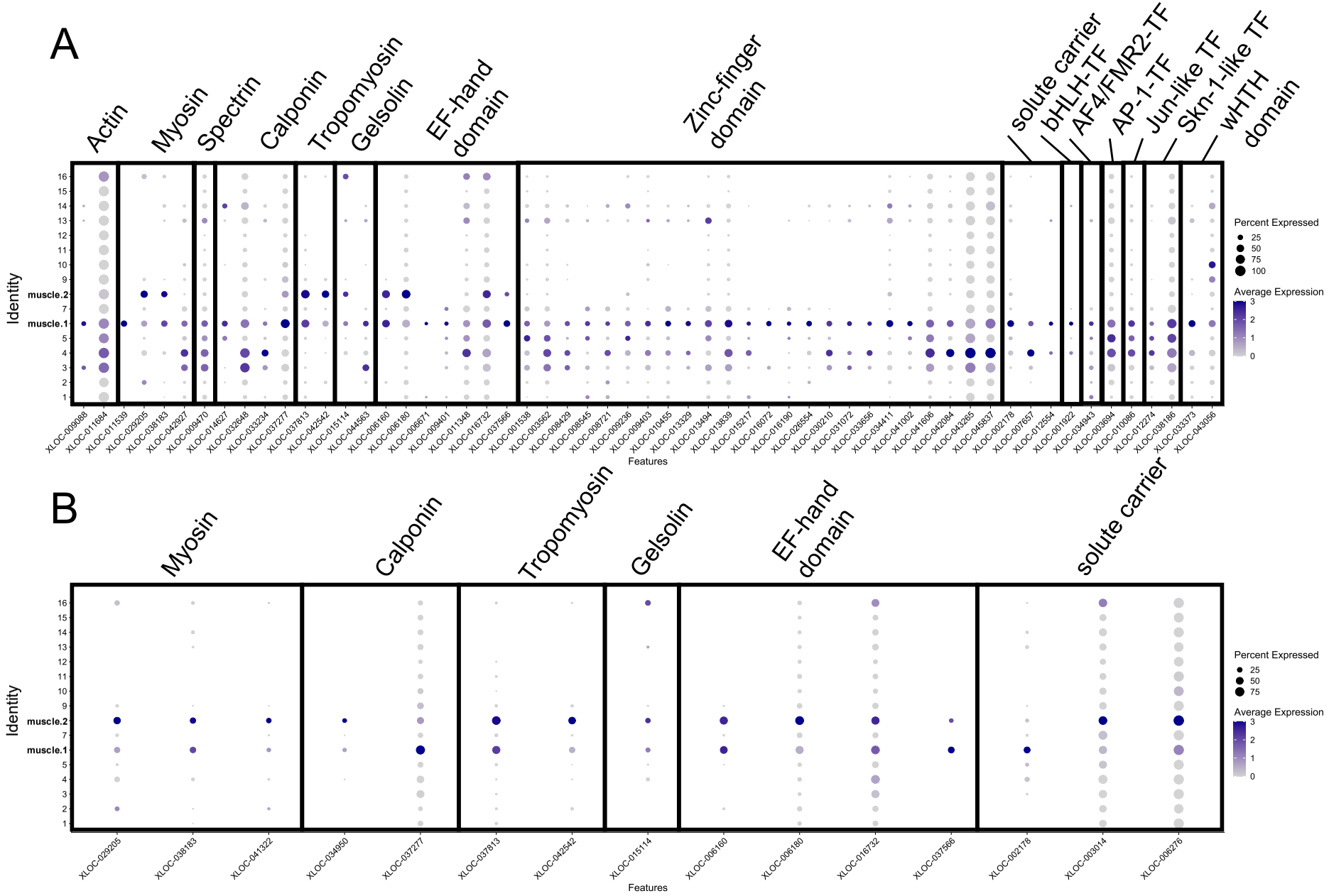
A
Actin
Myosin
Spectrin
Calponin
Tropomyosin
Gelsolin
EF-hand domain
Zinc-finger domain
solute carrier
bHLH-TF
AF4/FMR2-TF
AP-1-TF
Jun-like TF
Skn-1-like TF
wHTH domain
Identity
muscle.2
muscle.1
Features
Percent Expressed
25
50
75
100
Average Expression
3
2
1
0
B
Myosin
Calponin
Tropomyosin
Gelsolin
EF-hand domain
solute carrier
Identity
muscle.2
muscle.1
Features
Percent Expressed
25
50
75
Average Expression
3
2
1
0

Fig. 11: Muscular gene profiles of the two putative striated muscle clusters, derived from the differential gene expression analysis. The names of the genes are based on best BLAST hits. **A**: Gene composition of cluster muscle.1. Seven distinct structural proteins are found in this cluster, including two actins, four myosins and one spectrin. Two tropomyosins and gelsonins each, as well as four genes encoding for gelsolin make up the regulatory protein complement of this cluster. Additionally, four proteins containing an EF-hand domain and 25 genes encoding for proteins with a zinc-finger domain were found. Furthermore, three mitochondrial solute carriers are present. The transcription factors (TF) are made up of one basic helix-loop-helix (bHLH)-domain containing TF, five additional TFs. Finally, two likely TFs were also found, as these genes encode, among others, for a winged helix-turn-helix (wHTH) DNA binding domain. The second muscle gene cluster muscle.2 (**B**) shares multiple genes with cluster muscle.1, such as two of the three myosin genes in this cluster, both tropomyosins, and the only gelsolin found here. Further similarities are found among the EF-Hand domain containing proteins, where two of the four genes found in muscle.2 are also present in other striated muscle cluster, as well as one of three solute carrier proteins from muscle.2 being found in both clusters.

However, while in two genes encoding for actin were found in cluster muscle.1, no such gene was found to be present in muscle.2. This cluster also did not contain any genes with zinc-finger or spectrin homology domains. Most of the myosins, tropomyosins and calponins were found to have a very specific expression pattern confined to both striated muscle clusters. Furthermore, it is noteworthy that six transcription factors (TFs) and two probable TFs, based on the presence of winged helix-turn-helix (wHTH)-domains, are found in muscle.1, including one bHLH-TF. However, no TFs were found in cluster muscle.2.

All genes expressed *in-silico* in the putative striated muscles clusters were then subjected to the same GO-filtering pipeline described above. This was done to identify possible targets for subsequent functional studies on striated muscle function in *Clytia*. 44 genes of the muscle clusters were found to be associated with bilaterian sarcomere assembly GO-terms (supplementary Table S18).

3.2 Onset of striation in medusa buds and electroporation assay

3.2.1 Striated muscles appear to be formed in the developing medusa bud

This study additionally aimed for the identification of the timepoint of striated muscle development during *C. hemisphaerica* medusa formation. This was done to lay the foundation for future functional studies on sarcomere assembly by interfering with genes responsible for this function during striated muscle formation. As freshly hatched medusae are already able to swim freely through the medium and were found to possess striated muscles (Fig. 5), the formation of striated muscle types was expected to commence in early developmental stages of medusa bud formation.

Therefore, medusa buds growing in the gonozooid were stained with phalloidin and the expression pattern of genes identified as being expressed in striated muscles (listed in Fig. 8) was investigated by WMISH.

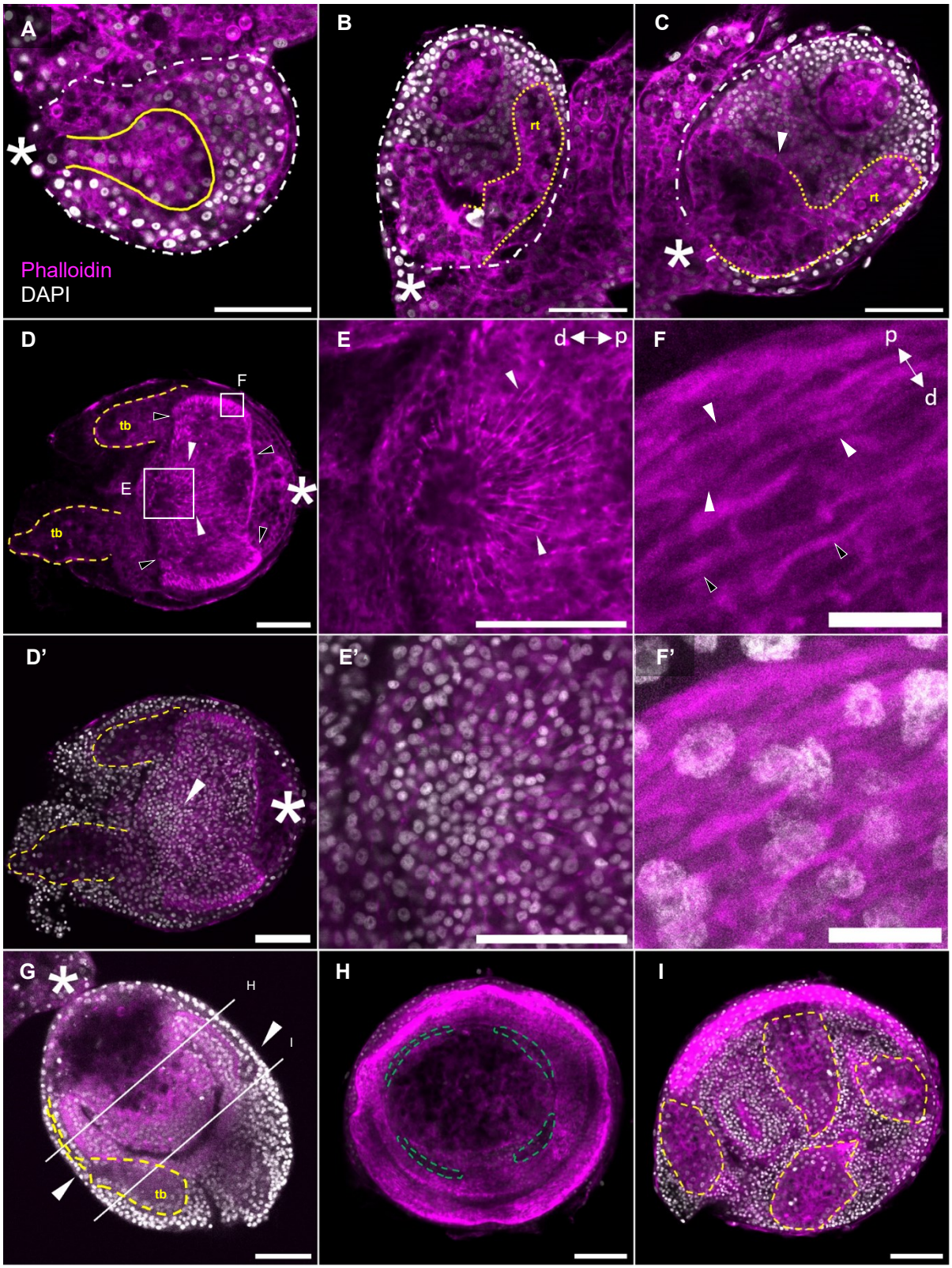

Fig. 12: Single confocal slices of phalloidin stainings of different developmental medusa stages in a gonozooid. **A, B, C, D, G**: lateral views of developmental stages from least to most developed medusa bud. **A:** Very early medusa bud (white dotted outline), still attached to the stalk of the gonozooid. Here, the early location of the endoderm (yellow outline) is in the center of the bud. **B:** Slightly more advanced medusa bud (white dotted outline), from the same gonozooid as **A**. Early radial tubes (yellow dotted line, rt) can be seen. **C:** More advanced medusa bud, taken from the same gonozooid as **A** and **B**. The rt appear more defined, and the manubrium (white arrowhead) grows more outward than in the earlier stages. **D:** Late-stage medusa bud. A belt-like structure appears in the middle of the animal. From the entocodon placed in the interspace of the rt, fibers appear to radiate (**E**, white arrowheads) into a belt-like structure (black arrowheads). Some of these fibers might have a striated appearance (**F**, white arrowheads) while others orientated in the same direction lack obvious striation (**F**, black arrowheads). **D'-F'**: Images **D-F** with the DAPI channel included. This shows that the "radiation patch" is densely populated with nuclei (**D'**, white arrowhead). **G:** Similar stage as **D**, different plane. The manubrium grows even more outward, while the radial tubes appear to start to differentiate into tentacle bulbs (tb, yellow outline). The tentacle bulbs seem to be separated from the radial tubes through a constriction (white arrowheads). **H:** Proximal-sided slice through the polyp of **G**. Parts of the entocodon cross (green dotted outline) are still visible. **I:** Distal-sided slice through the polyp of **G**. The localization of the tentacle bulbs (yellow dotted outline), which differentiated from the early rt, is rotated 45° relative to the entocodon cross. Asterisks denote the proximal (p) end of the medusa buds. Scale bars**:** 50 µm (**A-E**, **G-I**), 10 µm (**F**).

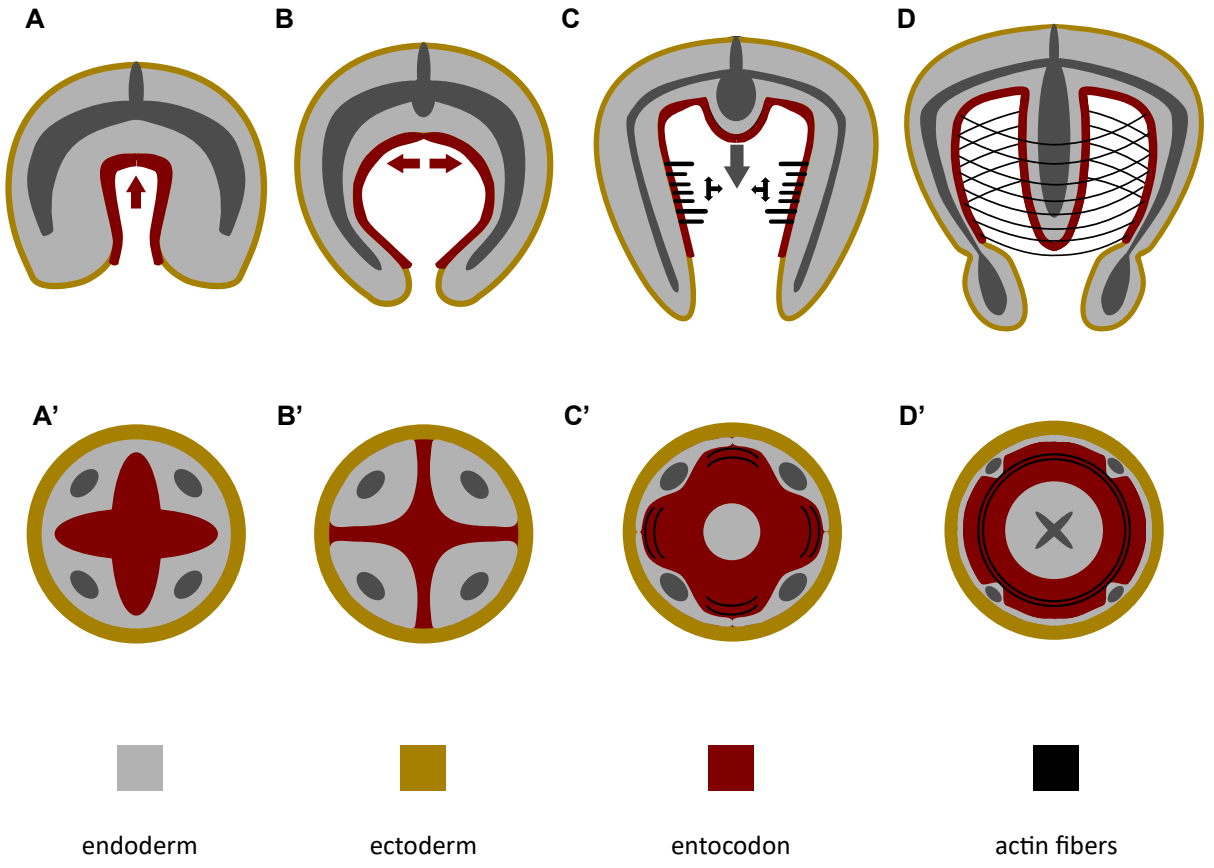

Fig. 13: Schematic drawings of muscle formation in *Clytia* medusa buds. Drawings based on results visible in Fig. 12, with information of tissue identity also based on Kraus (2013). **A-D**: Lateral view, **A'-D'**: top-down view. Ascending development from left to right. Note that medusa bud stages are not drawn to scale. Arrows show changes in localizations of the corresponding tissue. Possible muscle striation was found during the transition from **C** to **D**.

The medusa buds could be clearly identified (Fig. 12). In very early medusa buds, the entocodon is positioned towards the distal end of the polyp with the endoderm taking up most of the central space of the medusa bud (Fig. 12A). As the medusa develops, the entocodon moves proximally towards the center of the animal while the endoderm, which starts to develop into four radial tubes, moves outward and forms a cage-like shape (Fig. 12B, C; Fig. 13A, B). The space in between the radial tubes is filled by a structure described earlier as the entocodon cross (Kraus, 2013). Continuing development, the radial tubes appear to elongate, and the early manubrium starts to protrude the inner portion of the proximal side (Fig. 12C; Fig. 13B, C). At this point, four patches at the tips of the entocodon cross start to form a belt-like structure located in the middle of the medusa bud through outward radiation originating in these patches (Fig. 12D-F; Fig. 13C'). These patches seem to be rotated 45° relative to the location of the developing tentacles (Fig. 12G-I; Fig. 13B', C'). The belt-like structure appears to thicken and becomes more prominent as the polyp continues to grow and structures resembling fibers orientated circumferentially to the elongated proximal-distal axis of the bud become visible (Fig. 12F; Fig. 13D). Some of these fibers appear striated, however, due to resolution limitations, this could not be conclusively verified. Interestingly, other fibers orientated in the same direction lack the apparent striation (Fig. 12F). This was not observable in free-swimming medusae, where all actin fibers in the circumferential orientation were found to be striated (Fig. 5).

Gene expression of striated muscle-related genes can be detected in early medusa stages. However, it follows a different pattern than detectable by phalloidin staining. In very early stages, comparable to Fig. 12A, where the entocodon is starting to move inward and the endoderm is in the center of the animal, no gene expression of any gene associated with striated muscles can be detected (Fig. 14A; Fig. 15A). As soon as the endoderm forms the four radial tubes, four patches or spots arranged in a cross-like pattern can be observed (Fig. 14B, B'; Fig. 15B). These spots are in the entocodon situated in the interspace between the radial tubes (Fig. 15B'). Following development and elongation of the medusa bud, the spots inside the entocodon cross stretch and appear to be ovoid-shaped while retaining the cross-like arrangement visible in earlier stages (Fig. 14C; Fig. 15C). They then appear to grow thinner, but grow outwards toward each other, eventually forming a ring circumferential to the polyp primary axis (Fig. 14D; Fig. 15D). From this structure, the gene expression pattern also protrudes

towards the distal end of the medusa bud and forms a ring structure which will likely give rise to the future velum of the medusa, derived from a structure called velar plate (Kraus 2013, Fig. 14E).

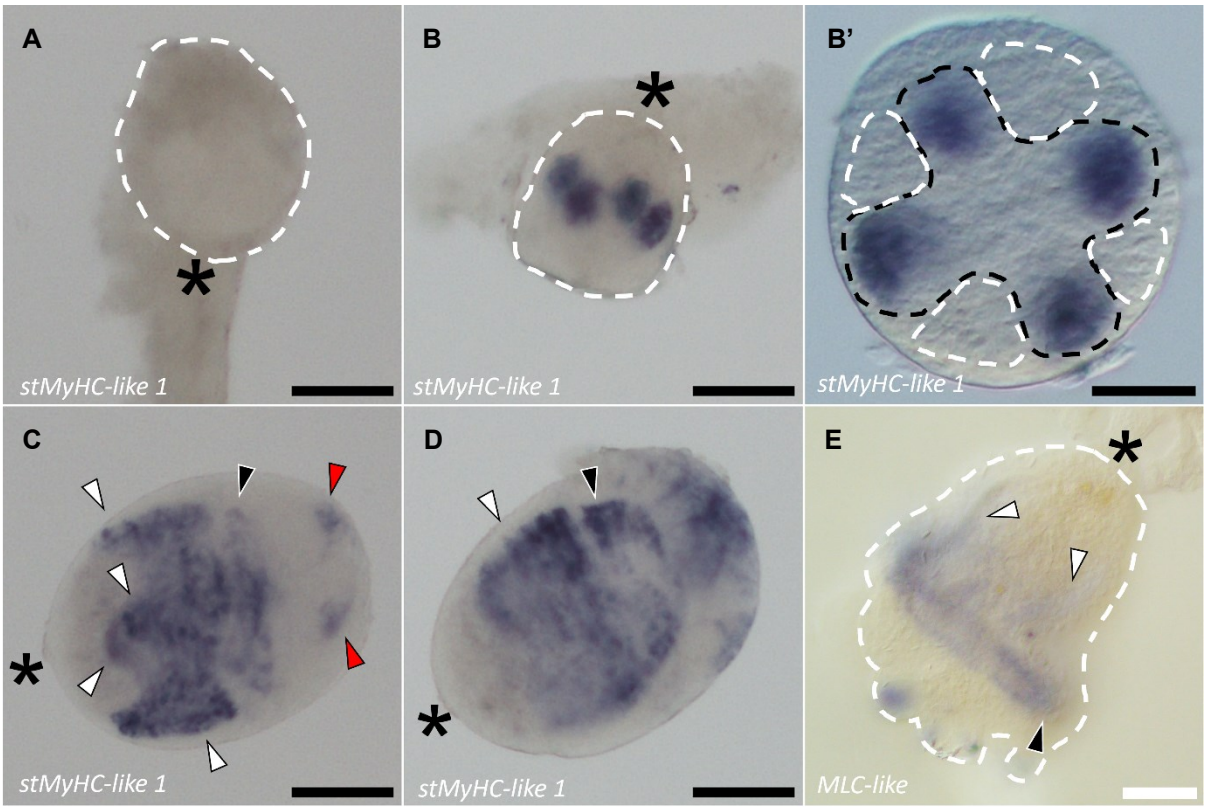

Fig. 14: Expression patterns of striated muscle marker genes during the development of medusa buds in a gonozooid. **A:** Very early medusa bud, lateral view. No gene expression visible. **B:** More advanced bud, lateral view. Four patches of *stMyHC-like 1* expression are in the entocodon. **B':** Same stage medusa bud, oral view, showing the positioning of *stMyHC-like 1* expression in a cross-like pattern. Black outline shows the location of the entocodon. White outline denotes the location of the radial tubes. **C:** Lateral view. Continuing development, the four expression patches (white arrowheads) elongate in the proximal-distal axis and appear to grow together, forming connections. Expression likely forming the velar plate (black arrowhead) can be seen. Expression in the tentacle bulbs is also visible (red arrowheads) **D:** Lateral view. The initial patchy appearance of gene expression is lost and instead, ar expression belt forms circumferential to the medusa bud (white arrowhead). The velar plate (black arrowhead) continues to move towards the distal end. **E:** Lateral view, *MLC-like* expression. Medusa bud shortly before detaching from the gonozooid stalk. The circumferential expression belt (white arrowheads) appears to be thinner than in the earlier expression stages and moves towards the periphery. The velar plate (black arrowhead) forms a ring towards the distal opening of the medusa bud, probably reflecting the velum of the medusa. Asterisks denote the proximal side of the medusa buds. White dotted outlines show the location of the medusa bud if they are still attached to the gonozooid stalk. Scale bars: 50 µm (**A**-**E**), 25 µm (**B'**)

During the last stages of medusa development, expression in both the subumbrella and velum are clearly distinguishable (Fig. 14E). Gene expression of *MLC-like*, *stMyHC-like 1* and *stMyHC-like 2* followed a similar expression pattern in the observed medusa buds (supplementary Fig. S2).

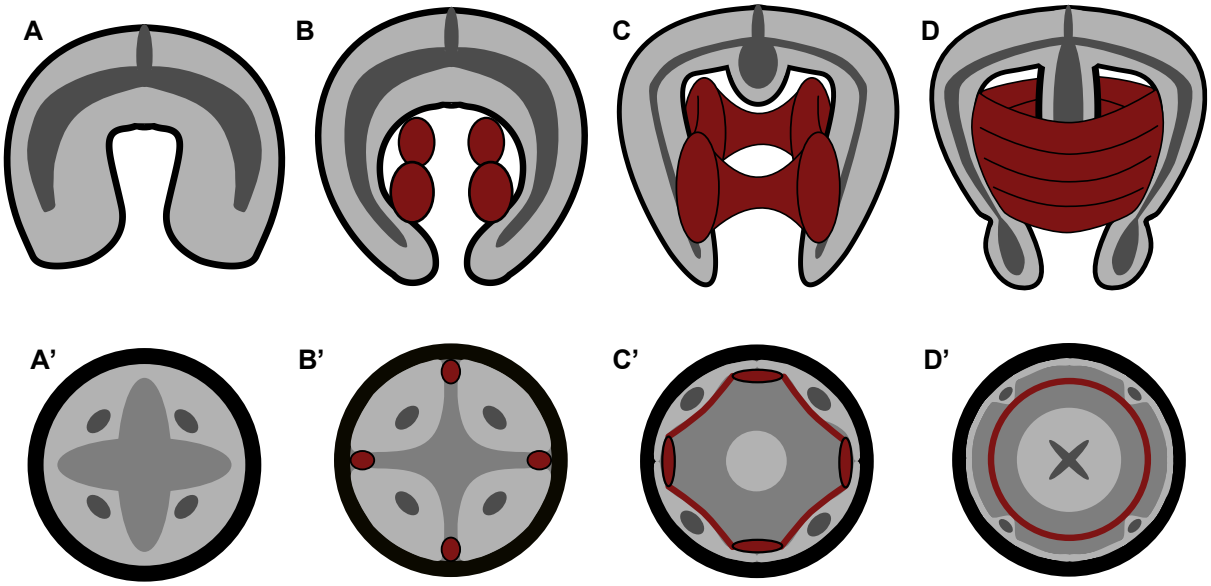

Fig. 15: Schematic drawings of *stMyHC-like* and *MLC-like* expression (dark red) in medusa buds. **A-D**: lateral view, **A'-D'**: top-down view. Ascending development from left to right. Note that medusa bud stages are not drawn to scale.

3.2.2 Electroporation of gonozooids is survivable, but not viable for delivery

It was suspected that the theca of the gonozooids might interfere with the electroporation by blocking the probe from reaching the medusa bud. Therefore, three different treatments were carried out to test whether medusa can grow and survive without being contained in the thecae. The treatments were a control group, comprised of polyps cut out of the stolon but otherwise untouched. A second group was made up of polyps with the lid removed, but the buds were still inside of the theca and still in contact with the leftover stolon. The third group had the buds completely removed from both theca and stolon, but, unless accidentally detached, still in contact with the gonozooid stalk. The three groups were then placed in petri dishes and survival rate was recorded over the course of multiple days (Fig. 16). No significant differences in the survival rate were observed between the three groups, medusae capable of swimming and feeding were found in all treatments with a survival rate of at least 50% recorded in all treatments seven days after treatment (Fig. 16), suggesting that the removal of the theca did not harm the survival in a significant way.

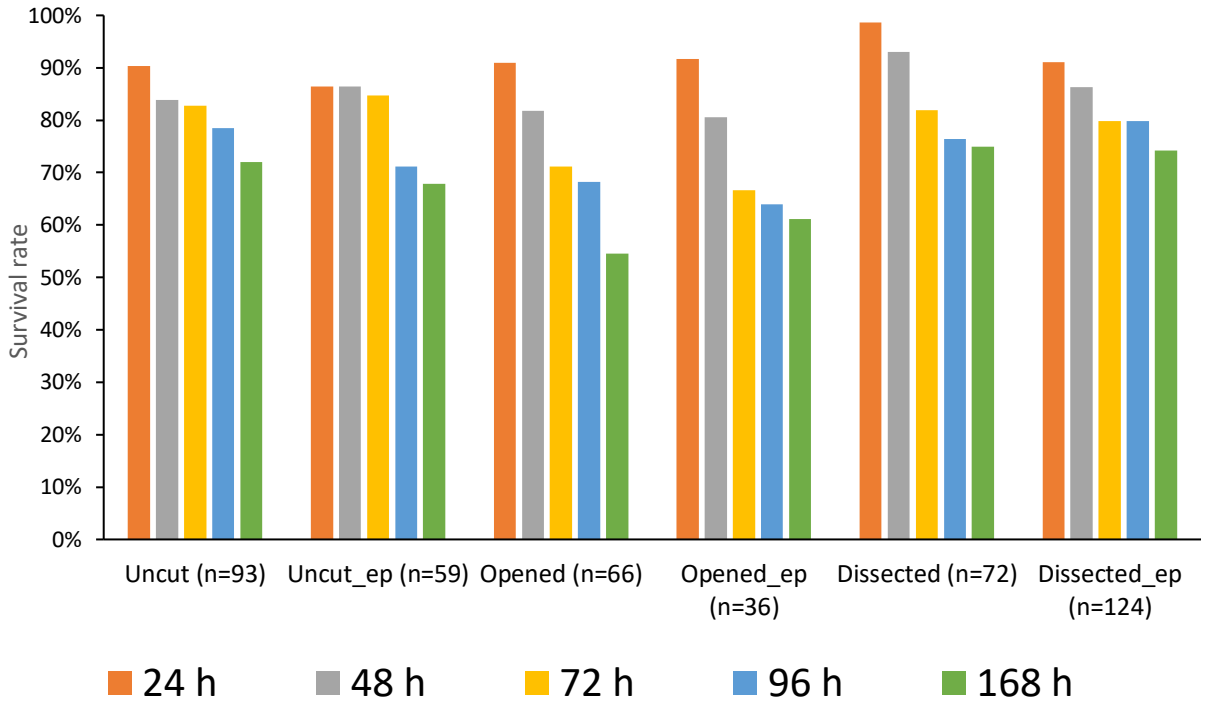

Fig. 16: Survival rate of *C. hemisphaerica* gonozooids after removal from the colony and electroporation, recorded over the course of seven days (168 h). The survival rates from 24 h onwards always show the proportion of medusa buds initially recorded at 0 h (immediately after treatment) which was able to grow into swimming medusae. n points to the number of medusa buds counted after at 0 h. Uncut corresponds to the group separated from the stolon, opened is the group with the removed lid and dissected described the treatment group with the medusa buds completely removed from the theca. The _ep addition denotes data from the respective treatment group after electroporation.

Furthermore, the endogenous GFP expression appeared to be unaffected by the electroporation procedure or treatment (Fig. 17A, D). However, it was observed that not all buds were developing into medusae, yet no significant difference between the groups was recorded. To test whether gonozooids survive electroporation, all three groups were subjected to a single electroporation pulse without any Dextran followed by recording of survival rates (Fig. 16). Again, no significant differences between the groups were observed, hence, all gonozooids had their thecae and stolon removed for all further electroporation experiments. First, it was examined if a tracer can be delivered into the gonozooid tissue by electroporation and how long the signal of the tracer is detectable. To this end, gonozooids prepared as described above were suspended in a solution of 15% Ficoll in FSASW and 2% Dextran-568 were added. The polyps were electroporated within 5 mins of addition of the Dextran, and immediately after washing out excess Dextran, they were screened for fluorescent signals.

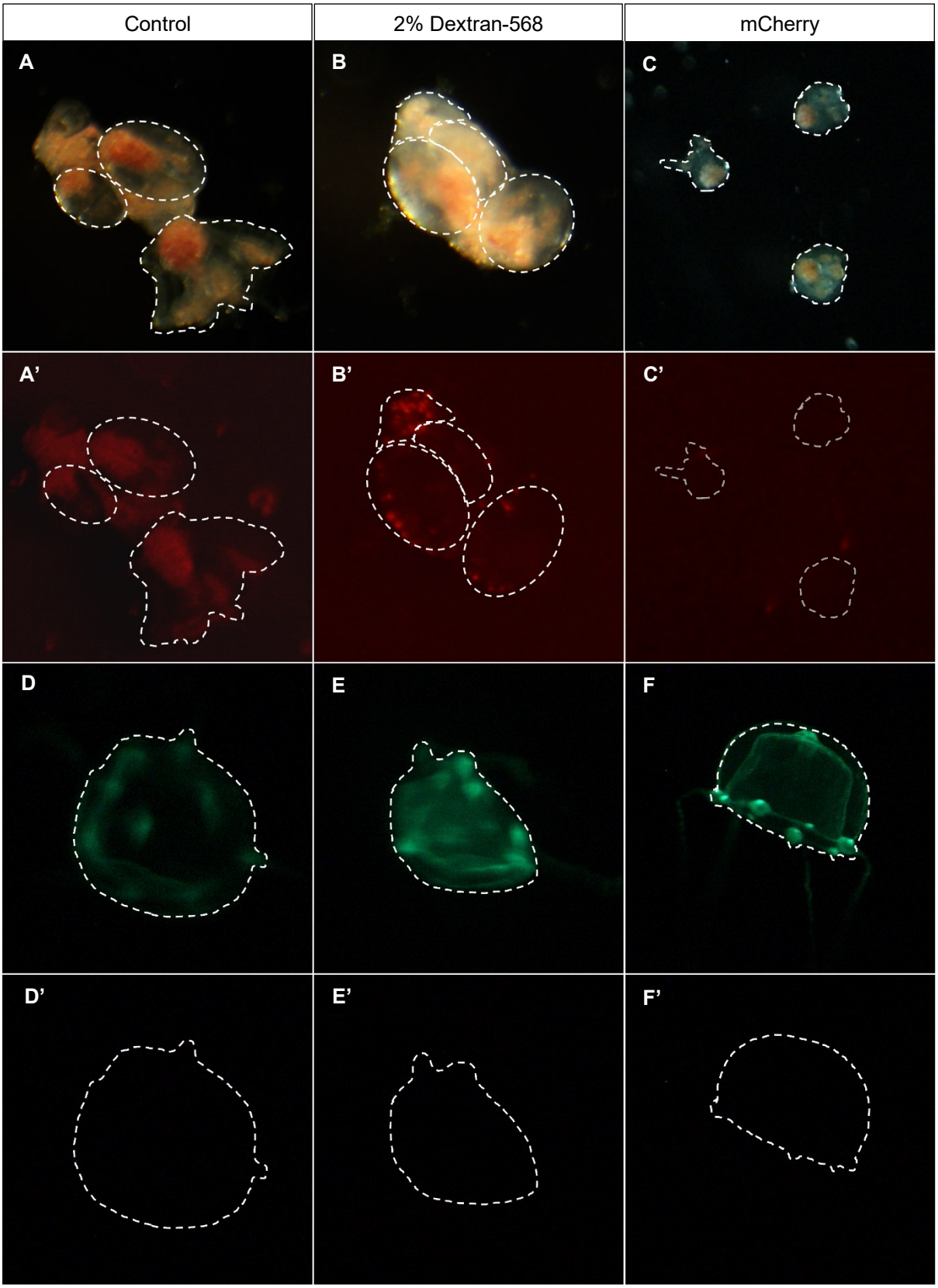

Fig. 17: *C. hemisphaerica* gonozooids after electroporation and their development into medusae. **A-C:** Brightfield images of the gonozooids without a tracer (control), with Dextran-568 and with mCherry RNA, respectively, immediately after electroporation. **A'-C':** Images taken with the RFP channel of the same gonozooids to confirm the presence or absence of a red tracer signal. **D-F:** GFP-channel images of the gonozooids after one night of development (**D** & **E**) or after 3 days (**F**). The medusae were able to swim and localization of the endogenous GFP signal followed a normal localization pattern. **D'-F':** RFP channel of the same medusae. White outlines denote the location of the medusa buds and grown medusae.

A strong signal could be observed on the outer tissue of the medusae buds (Fig. 17B, B'). However, after the buds have developed into medusae, no further signal could be detected (Fig. 17E, E'). This observation did not change with different concentrations of Dextran-568 in the medium. A second experimental setup was prepared, this time not Dextran-568 but mRNA encoding for mCherry protein was electroporated into the medusa buds in the same matter as described above, with a final mRNA concentration of 1 µg/ml in the electroporation mix. No signal was visible in the gonozooid stages immediately after electroporation (Fig. 17C, C'). The animals were screened after multiple days after they developed into medusae, giving sufficient time for mCherry protein to accumulate to be detectable. However, although the medusae survived and were able to swim and feed, no mCherry signal was detectable (Fig. 17F, F'). The development of the medusae was followed over the course of one week, but no observable mCherry signal was detectable at any time.

3.3 The umbrella appears to expand by allometric growth

As seen in the phalloidin and WMISH images of *C. hemisphaerica* medusae, the localization of striated muscles varies throughout medusa growth, which could be a result of allometric growth of the umbrella. EdU pulse-labeling stainings were performed to investigate whether the umbrella expands through uniform cell division or by allometric growth in specific growth zones. In *C. hemisphaerica* medusa buds, a belt-like EdU signal was detected, which was in the middle of the proximal-distal axis of the medusa bud (Fig. 18A, B). Apart from this structure, no other accumulated S-phase cells became apparent in medusa buds. In juvenile medusae, EdU staining is found mostly in the tentacles and tentacle bulbs (Fig. 18C; Fig. 19A, B). In-between the four tentacle bulbs of juvenile medusae, in the areas where the secondary tentacle bulbs grow, a strong EdU signal can also be found (Fig. 19B). Furthermore, the tip and the lateral side of the manubrium show high levels of EdU staining (Fig. 19A, C, D). The staining in the manubrium appears to be very uniform and extends into the four radial canals (Fig. 19C). In the subumbrella, however, the staining is mostly found in the regions where the gonads start to grow, with staining in the rest of the subumbrella being detectable in only a few cells (Fig. 19A).

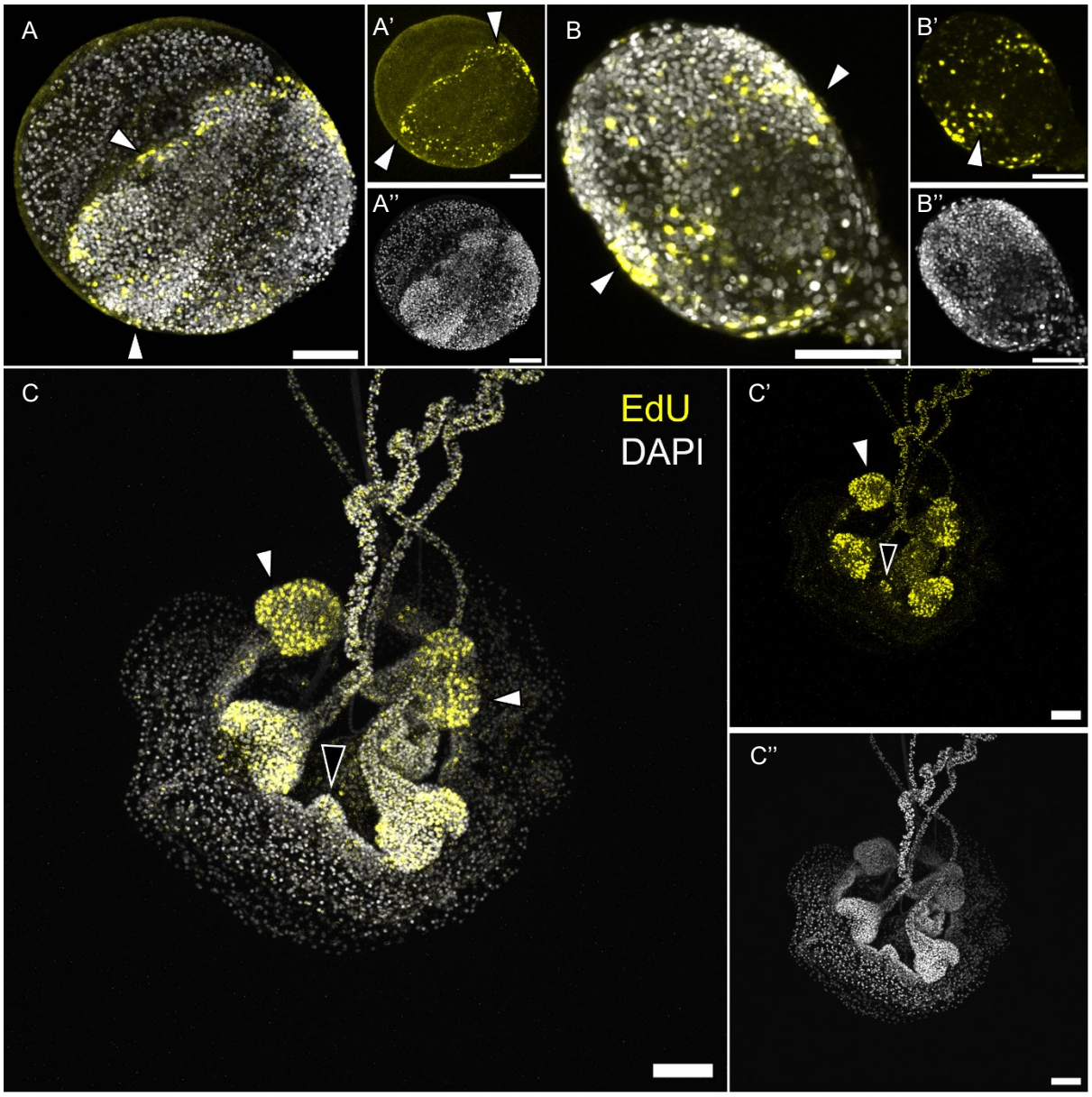

Fig. 18: EdU staining of middle- to late-stage medusa buds. **A** and **B**: lateral view of medusa buds mid-development after a 30 min EdU pulse. Here, EdU-positive cells form a ring or belt-like structure (white arrowheads) circumferential to the proximal-distal axis of the buds. This structure appears to be located within the ectoderm. **C**: Semi-lateral view of a very late-stage medusa bud, very shortly before detaching from the colony. At this stage, the major structures such as tentacle bulbs, tentacles and the umbrella are all clearly identifiable. Cell division is very pronounced in the tentacle bulbs (white arrowheads) and at the location where the secondary tentacle bulbs are beginning to form (black arrowheads). In the subumbrella, very little EdU signal can be found. Scale bars: 50 µm.

At the rim of the subumbrella, in the area where the velum is located, EdU-positive cells form a ring circumferential to the opening of the medusa, however, it does not become apparent whether these cells arise from the tentacle bulbs or if they were already situated in the velum area when they entered the cell division cycle (Fig. 19A, F). Furthermore, some of these cells have an elongated appearance, which would be indicative of mis-labeled nematocysts.

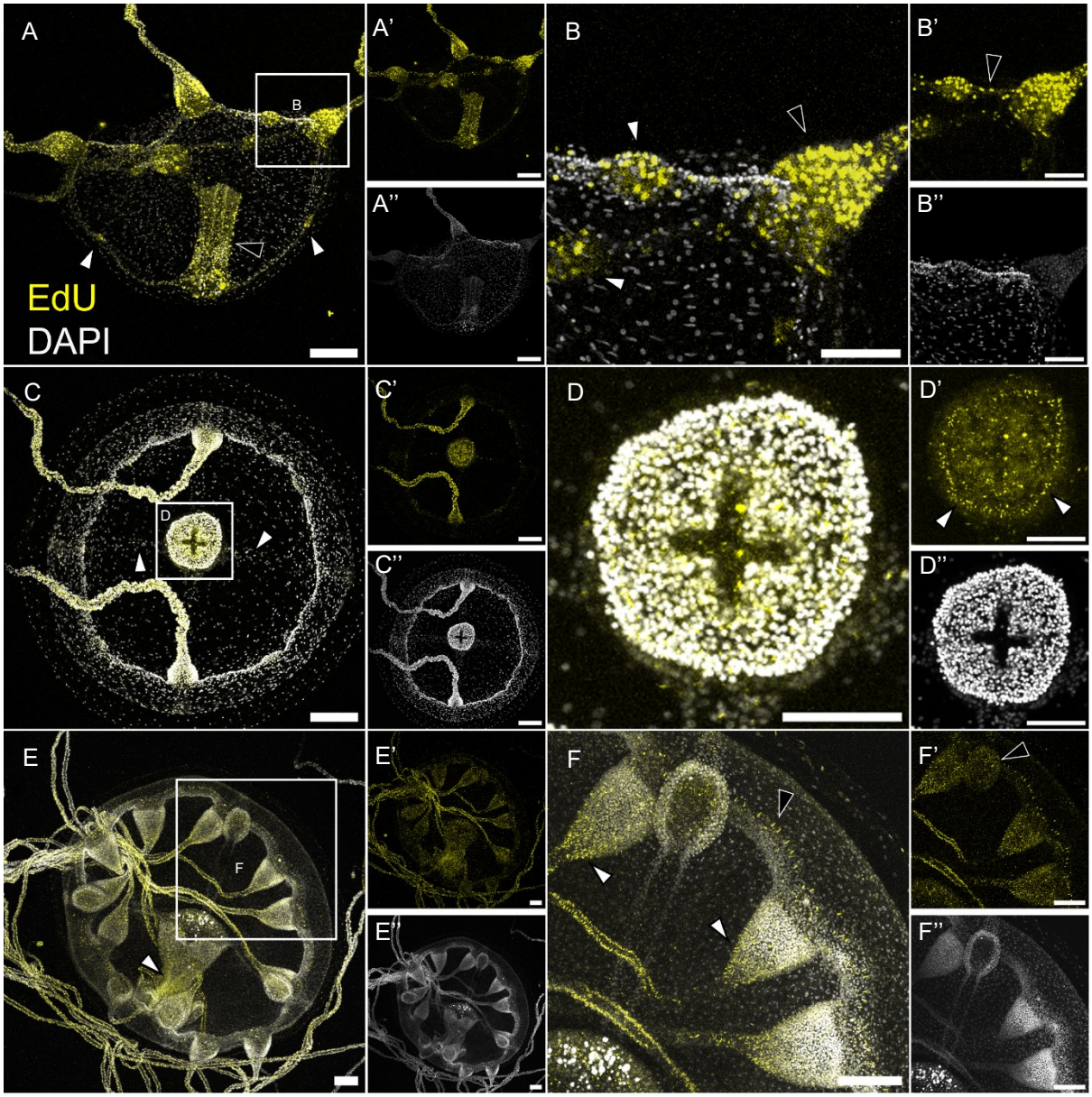

Fig. 19: EdU staining in juvenile and adult medusa stages of *C. hemispharica*. **A**: Lateral view of a juvenile medusa. The EdU signal is very pronounced in the tentacle bulbs (**B**, black arrowhead), in the secondary tentacle bulbs (**B**, white arrowheads), at the location of the future gonads (white arrowheads) and along the manubrium (black arrowhead). The subumbrella appears mostly void of EdU-positive cells (also visible in **B**), although cell nuclei are abundant in this region. In the velum and at the rim of the umbrella, close to the distal opening, some EdU-positive cells can be seen (**B'**, black arrowhead). The EdU signal at the velum-bell rim area appears to extend circumferential around the entire animal. **C**: Oral view of a juvenile medusa. Note that during mounting, two tentacle bulbs with their tentacle accidentally became detached. This view highlights cell division at the manubrium tip (enlarged in **D**) and shows some EdU signal in the radial canals (white arrowheads). At this location, however, no aggregation of cells was detected in the DAPI channel, as it would be found at the growth location of the gonads (**C''**). **E**: Oral view of an adult medusa, highlighting fully developed gonads and numerous tentacle bulbs. Consistent with juvenile medusae, the EdU signal was mostly found in the tentacle bulbs (**F**, white arrowheads), in the gonads (**F'**, black arrowhead) and in the manubrium (white arrowhead). Again, as found in earlier stages, little to no signal was found in the subumbrella, except for a band of EdU-positive cells in the velum-rim area (**F**, black arrowhead). Scale bars: 100 µm (**A**, **C**, **E**, **F**), 50 µm (**B**, **D**)

The EdU signal in adult medusae follows mostly the same pattern, with strong staining in the tentacle bulbs, manubrium, and gonads (Fig. 19E, F). Overall, these results suggest that cell proliferation occurs less in the subumbrella than in other structures, which could possibly indicate allometric growth in the expansion of the medusa, yet as some apparent mis-labelings were recorded, these results are thus far inconclusive.

4 Discussion

Preliminary differential gene analysis done prior to this study by Oliver Link (unpublished) revealed that two clusters likely contain muscles in our dataset, which were termed muscle.1 and muscle.2. To validate the identity of the putative muscle clusters of our dataset, four WMISH probes were generated. It is noteworthy that no gene was found to be expressed in cluster muscle.2 only, with all potential marker genes for this cluster showing some *in-silico* expression in cluster muscle.1. Upon closer inspection, it was found that two of these genes (*stMyHC-like 1* and *2*) have been used in previous studies as marker genes for muscles in the velum and subumbrella (Chari et al., 2021; Kraus, 2013; Steinmetz et al., 2012). As *stMyHC-like 2* shows a strong *in-silico* expression pattern in both putative muscle clusters with little expression in other clusters, this reaffirmed the cluster identity in our dataset. The other two genes (*MTPN-like* and *MLC-like*) were thus far not used as WMISH probes for *C. hemisphaerica*. Except for *MTPN-like*, which is exclusively expressed in cluster muscle.1, the staining pattern in medusae of our probes overlaps with the location of subumbrellar and velar muscles as seen in the phalloidin staining. Furthermore, while *stMyHC-like 2* shows an expression pattern throughout the entire bell of a juvenile medusa, the staining follows exclusively the circumferential orientation as seen with phalloidin. Also, no staining was found around the base of the manubrium, an area which was found to be populated with radial smooth muscles in phalloidin images. This indicates that this probe only stains striated and not smooth muscle fibers in the medusa subumbrella. However, as previously reported (Kraus, 2013) and as seen in this study, the subumbrellar smooth muscles are thinner in appearance than striated muscle fibers. Thus, it is possible that staining in radial smooth muscles was too faint to be identified or that the smooth muscle fibers became damaged during the *in-situ* process. Both *stMyHC-like* probes, however, did not exclusively stain striated muscles but were also found in the tentacle bulbs and along the manubrium, consistent with previous findings (Chari et al., 2021;

Kraus, 2013; Steinmetz et al., 2012). While having a similar *in-silico* expression pattern to *stMyHC-like 2*, *MLC-like* was not found to be expressed in the tentacle bulbs or manubrium *in-situ*. Instead, it was being found only in the velum of adult medusae, with the expression overlapping the location of striated muscles in this tissue identified by phalloidin. Whether this gene is also expressed in the subumbrella of juvenile medusae is unclear, as the probe did not show any staining while being used on this stage. Kraus (2013) reported that a *myosin light chain kinase* gene was expressed exclusively in striated muscles and not in other tissues, yet we were unable to identify this gene in our scRNAseq data. However, the expression patterns of the *MLCK* probe from the published data and of *stMyHC-like 1* and *2* as well as *MLC-like* presented here are very similar in developing medusa buds, showing the same tetramerous expression pattern. This further argues that our probes are expressed in striated muscles, contributing to the validity of our two muscle clusters. As published in an earlier study (Chari et al., 2021), *C. hemisphaerica* shows the presence of two sets of striated muscles. According to their data, one of the striated muscle populations is associated with the velum and one striated muscle population contains the transcriptomes of the subumbrellar striated muscles. However, when using the pre-published set of striated muscle marker genes and visualizing their expression pattern *in-silico*, the marker genes showed strong expression in both of our putative muscle clusters. This argues that striated muscles of velum and subumbrella share a very similar set of genes and are could likely be confined to one cluster in our dataset with the other cluster being a developmental stage, as our dataset was derived from a juvenile medusa and not an adult animal as used for their data. Furthermore, not all clusters in our dataset could be putatively annotated through comparison with the published marker genes (Chari et al., 2021), which likely also stems from different medusa stages used for the scRNAseq. If striated muscles are confined to one cluster in our dataset, the other cluster likely contained smooth muscles based on the WMISH pattern of *MTPN-like*. This gene shows a very specific *in-silico* expression pattern, being expressed in cluster muscle.1 only. WMISH data shows this gene is not expressed in either population of striated muscles but instead briefly in the manubrium during development before becoming undetectable in mature medusae. This correlates with the findings of both *stMyHC-like* probes, which stained the manubrium while also being expressed in cluster muscle.1, although the staining pattern of *MTPN-like* and *stMyHC-like* was different in the manubrium. However, whether the WMISH results of *MTPN-like* are accurate is

unclear, as I was unable to produce more probes with a similar *in-silico* expression and no literature using this or similar probes of the manubrium was found. If the WMISH data does indeed represent the expression pattern of *MTPN-like*, this would argue for cluster muscle.1 not to contain striated muscles nor being a developmental stage. Instead, this cluster contains smooth muscles responsible for manubrium motility, which are reported to be fast contracting (Kraus, 2013). In conclusion, cluster muscle.2 was identified with high confidence as containing striated muscles from velum and subumbrella, probably not being specific to either. The identity of the muscle.1 cluster was more obscure, yet based on the data presented here, this cluster likely contains smooth muscles of the manubrium and possibly also of the subumbrella. Therefore, future studies should try to reproduce WMISH data with probes specific to cluster muscle.1, to also possibly identify smooth muscles of the subumbrella.

Both clusters muscle.1 and .2 contain multiple transcripts of genes which are annotated as being required for muscular function and contraction, however, most of the transcripts found in muscle.2 are also present in cluster muscle.1. They both share two myosin proteins, which, together with actin, forms the contractile complex of muscles cells (Boland et al., 2019). However, actin was only found in cluster muscle.1. As actin is a ubiquitous proteins found in virtually all eukaryotic cells (Xu et al., 2013), the absence of actin transcripts in most clusters highlights the limitations of shallow 10X scRNA sequencing as well as incomplete annotation of our dataset, which was also apparent by the lack of identified transcription factors in cluster muscle.2. Nevertheless, the annotations which are present give insight into the molecular profile of the putative striated muscle clusters. Two transcripts of tropomyosin were found to be very specifically expressed in clusters muscle.1 and .2. Tropomyosin is one of two principle regulatory proteins of muscle contraction and relaxation, the other being troponin (Boland et al., 2019). Concurring with previous studies, our dataset did not show the presence of troponins, which aligns with the finding that this protein is a bilaterian novelty and underlines the convergent evolution of striated muscles in bilaterians and non-bilaterians (Steinmetz et al., 2012). This extends to the structural titin protein, acting as an anchor connecting myosin to the z-disc, yet also not present in non-bilaterians (Boland et al., 2019; Steinmetz et al., 2012). Further genes found in these clusters include gelsolin, which is an actin-binding protein not exclusive to but often found in muscle cells (Khaitlina et al., 2013; Kwiatkowski et al., 1988). Interestingly, genes

annotated as calponin were found to be present in the striated muscle cluster. In Bilateria, muscular calponin is thought to be exclusively found in smooth muscle cells (Hsieh and Jin, 2023; Royuela et al., 1996), where it regulates the ATPase activity of myosin (Ferjani et al., 2010). Thus, the identification of calponin in striated muscle clusters would further contribute to the analogous evolution of bilaterian and cnidarian striated muscles. However, whether the calponins found in this study are like bilaterian calponin and if they follow the same function is highly speculative and should be thoroughly investigated in the future. Potential targets for functional studies on the sarcomere assembly and maintenance were identified though GO-filtering with terms associated with bilaterian striated muscles and sarcomere assembly. However, only few of the GO-terms used for filtering were found to be present in our dataset. Most genes were associated with GO-terms such as protein binding, calcium-ion binding, and ATP-binding. Concurring with the previous finding, no GO-terms specific to Titin-binding, the Titin-Telethonin complex, and Titin z domain binding could be identified, inline with Steinmetz et al. (2012), highlighting that these proteins are likely absent in Medusozoa. Furthermore, no genes associated with either the z-disc, A-band, I-band, M-band, or more general terms such as muscle contraction, actomyosin, and sarcomere organization were found to be differentially expressed in our dataset.

Genetic tools for *C. hemisphaerica* are so far not as established as for other model organisms. As electroporation is a fast method with a high throughput of specimens, I tried to develop an electroporation protocol for the medusa-bud containing gonozooids of *Clytia*, which is the stage in which striated muscles are suspected to form. Investigation with phalloidin suggests that striation arises at around the same time when the tentacle bulbs become visible in the latter stages of development, shortly before detaching from the colony. However, expression of genes of medusa striated muscles can be found early on during medusa bud development before striation is visible, arranged in four patches. Also, it appears as if muscle fibers appear to originate from these patches through outward radiation. The findings concur with previous studies, which show that a tissue layer, called entocodon, forms by delamination from part of the ectoderm formed at the distal end of the medusa bud and eventually fills the interspace between the four radial tubes. At this point, it is referred to as entocodon cross, with the expression of muscular genes being found in four patches (Frey, 1968; Kraus, 2013; Kraus et al., 2015). After forming a belt-like structure, a certain degree of

striation can be seen. However, as resolution constraints do not allow for a conclusive result, this should be investigated further with higher-resolution imaging methods as presented here. Nevertheless, these findings indicate that striated muscles likely first have a smooth appearance and gain striation later, thus, sarcomere assembly takes place during medusa bud development. Provided that these ultrastructural changes are accurate and not the result of visual artifacts or imaging errors, this would further highlight differences in striated muscle development between Vertebrate and Medusozoa, as such changes were not observed in vertebrates (Gabella and Clarke, 1983). In another group of medusozoans, the Scyphozoa, striated muscles were found to originate from numerous actin-rich bundles. These bundles also appeared to elongate and broaden during their development and come into contact (Helm et al., 2015), yet the quadrant-based appearance of muscular development in the entocodon is unique to hydrozoans (Sinigaglia et al., 2020). However, the underlying principles of muscle formation in Hydrozoa and why it starts with four patches and not as a ring is thus far unknown. Previously, the entocodon of hydrozoans has been compared to the mesoderm of triploblasts, due to its location between ectoderm and endoderm, and because both structures give rise to striated muscles (Seipel and Schmid, 2005; Seipel and Schmid, 2006). Recently, however, this has been contradicted, placing the entocodon as an analogous structure to the mesoderm of triploblastic animals (Burton, 2008; Kraus, 2013; Kraus et al., 2015).

As striated muscles appear to be formed in the medusa buds, they are suitable for knockdown assays targeting striated muscle formation. Removal of the theca, which was expected to act as a barrier during molecule delivery, does not seem to impair the survival of the medusa buds over the course of four days. Furthermore, the gonozooids survive electroporation using the same parameters which are shown to be viable for larvae (Masuda-Ozawa et al., 2022). Using dextran as a control for the proof-of-principle of electroporation showed the molecule being delivered into the medusa buds, but it could not be detected after the medusa had developed. It was expected that for a successful knockdown, the knockdown agent would have to remain longer in the tissue allowing for it to be transcribed. Therefore, mRNA encoding for *mCherry* was electroporated into the medusa buds. The expression of mCherry protein, identifiable by red fluorescence, would indicate that a product can be delivered into the tissue and stays stable long enough for it to be transcribed, a prerequisite for

successful knockdowns. However, no expression of the gene was found in medusa buds or medusae. The application of electroporation on medusa buds was thus far not reported, yet a recent study has shown that electroporation of *C. hemisphaerica* planula larvae is a viable method for gene knockdown. It was demonstrated that the endogenous GFP expression can be reduced by introducing small interfering RNA molecules into the larvae (Masuda-Ozawa et al., 2022). The same study was further able to show that targeting *Wnt3* in the same matter results in defects in larval axis patterning, highlighting the potential of electroporation for functional studies. Whether this knowledge also translates to the more advanced medusa bud stage remains unknown, as Masuda-Ozawa et al. (2022) did not investigate whether the knockdown effect remains stable throughout continued development. Nevertheless, the insights gained from the dissection experiments and the ability of animals with their thecae removed to survive the electroporation show promising success and help form a basis for future experiments on gene knockdown through electroporation of developmental stages of *C. hemisphaerica*.

As observable by phalloidin and WMISH stainings it appears that the subumbrellar striated muscles undergo changes in their localization during medusa growth. Visually, it seems as if they are pushed towards the distal side of the medusae, with the space around the manubrium base eventually being populated solely by smooth muscles (Fig. 20). This concurs with WMISH stainings, which show subumbrellar striated muscle gene expression only during juvenile stages of development, being confined to the distal end with increasing age (Fig. 20). To determine umbrella growth and to find a possible explanation as to why striated muscles become situated towards the distal side, EdU staining was employed. This revealed growth areas in the tentacle bulbs and the manubrium, with EdU staining being virtually absent from the subumbrella except for a few cells. For this study, the specimens were pulsed for 30 mins with EdU, yet prolonging the pulse time to 24 h also does not change observation that the subumbrella contains less EdU-positive cells than the manubrium or the tentacle bulbs, which was shown in a previous study (Sinigaglia et al., 2020).

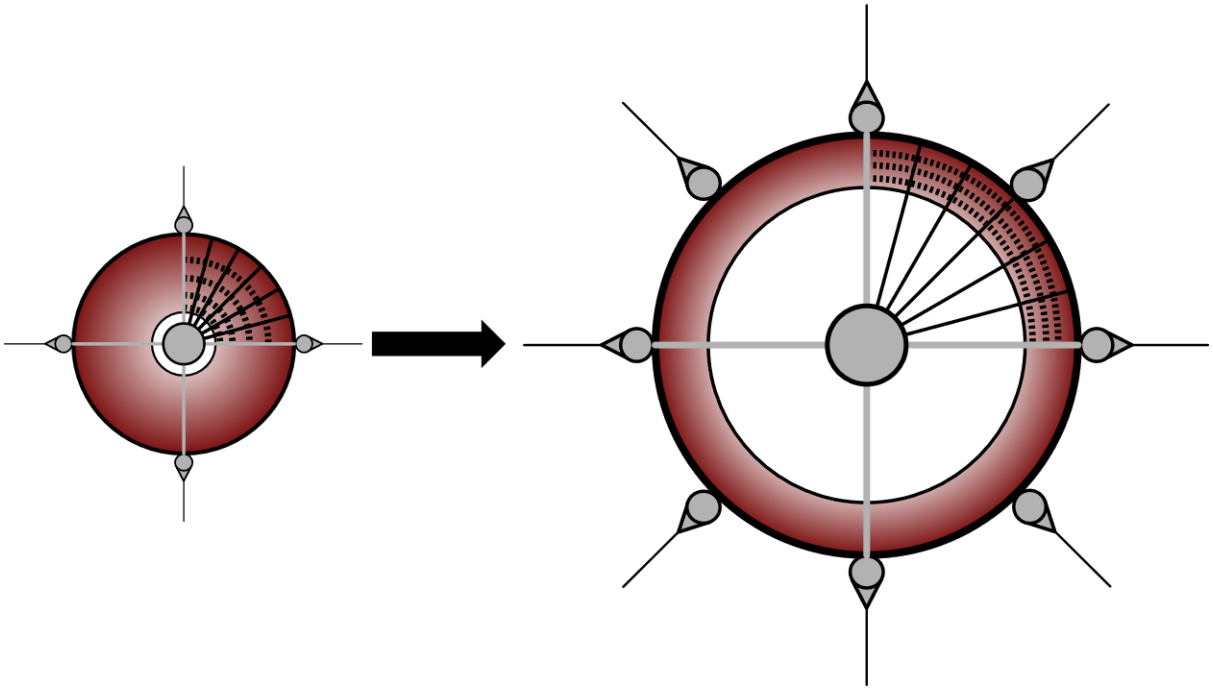

Fig. 20: Schematic representation of subumbrellar muscle localization during medusa growth. Muscles are drawn in one quadrant each. While smooth muscles (solid black line) are present throughout the entire subumbrella in both baby and adult medusae, striated muscles (dashed black line) become more outward and distally located in adult animals. This variability is also reflected in striated muscle gene expression patterns in the subumbrella (dark red). Figure is based on phalloidin and WMISH images.

However, in both the data presented here and in the published data (Sinigaglia et al., 2020), tentacles were found to be stained with EdU, in some cases having an elongated appearance. This would be indicative of a mis-labeling of nematocytes with EdU, thus, the results of the EdU staining presented here should be taken cautiously. Nevertheless, staining in the tentacle bulbs as well as the manubrium appeared specific to dividing cells, as they do not have the elongated appearance and showed to overlap with nuclei. Staining in these structures concurs with the finding that here, the pluripotent stem cells (also called i-cells) are harbored (Chari et al., 2021; Denker et al., 2008; Gold and Jacobs, 2013). Sinigaglia et al. (2020) also found that the four radial tubes play a central role in distributing i-cells throughout the animal, which could provide a possible explanation of the finding of EdU-positive cells in the location of the radial tubes in one of the samples of this study. These findings, although thus far not conclusive, indicate that the umbrella does not grow through uniform cell division but hint at the existence of growth zones with subsequent distribution of differentiating cells throughout the medusa body. Schmid et al. (1974) reported that that the umbrella of *C. hemisphaerica* indeed expands by allometric growth through a growth zone at the periphery of the bell. Thus, they concluded that the medusa umbrella expands by

addition of tissue to the umbrella margin rather than by growth and distribution through the manubrium or uniform cell division in the subumbrella. Combining this with observable changes in striated muscle localization, striated muscle cells might be produced in the periphery of the bell while more centrally located striated muscle cells are not maintained during bell expansion. However, this hypothesis is so far not investigated enough and thus should be subjected to further research. Possibly, a TUNEL-assay could be employed, which would mark apoptotic cells centrally in the umbrella, provided this hypothesis holds true (Gorczyca et al., 1993).

References

Amiel, A., Leclère, L., Robert, L., Chevalier, S. and Houliston, E. (2009). Conserved Functions for Mos in Eumetazoan Oocyte Maturation Revealed by Studies in a Cnidarian. *Current Biology* **19**, 305–311.

Boland, M., Kaur, L., Chian, F. M. and Astruc, T. (2019). Muscle Proteins. In *Encyclopedia of Food Chemistry* (eds. Melton, L., Shahidi, F., and Varelis, P.), pp. 164–179. Academic Press: Oxford.

Bouillon, J., Medel, M., Pagès, F., Gili, J.-M., Boero, F. and Gravili, C. (2004). Fauna of the Mediterranean Hydrozoa. *Sciencia Marina* **68**, 5–438.

Brunet, T., Fischer, A. H., Steinmetz, P. R., Lauri, A., Bertucci, P. and Arendt, D. (2016). The evolutionary origin of bilaterian smooth and striated myocytes. *Elife* **5**, e19607.

Burton, P. M. (2008). Insights from diploblasts; the evolution of mesoderm and muscle. *J Exp Zool B Mol Dev Evol* **310B**, 5–14.

Carré, D. and Carré, C. (2000). Origin of germ cells, sex determination, and sex inversion in medusae of the genus *Clytia* (Hydrozoa, Leptomedusae): The influence of temperature. *J Exp Zool* **287**, 233–242.

Chari, T., Weissbourd, B., Gehring, J., Ferraioli, A., Leclère, L., Herl, M., Gao, F., Chevalier, S., Copley, R. R., Houliston, E., et al. (2021). Whole-animal multiplexed single-cell RNA-seq reveals transcriptional shifts across *Clytia* medusa cell types. *Sci Adv* **7**, eabh1683.

Cole, A. G., Jahnel, S. M., Kaul, S., Steger, J., Hagauer, J., Denner, A., Murguia, P. F., Taudes, E., Zimmermann, B., Reischl, R., et al. (2023). Muscle cell-type diversification is driven by bHLH transcription factor expansion and extensive effector gene duplications. *Nat Commun* **14**, 1747.

Colgren, J. and Nichols, S. A. (2022). MRTF specifies a muscle-like contractile module in Porifera. *Nat Commun* **13**, 4134.

Craig, R. and Padrón, R. (2004). Chapter 7 Molecular Structure of the Sarcomere. In *Myology*, pp. 129–166.

Denker, E., Manuel, M., Leclère, L., Le Guyader, H. and Rabet, N. (2008). Ordered progression of nematogenesis from stem cells through differentiation stages in the tentacle bulb of *Clytia hemisphaerica* (Hydrozoa, Cnidaria). *Dev Biol* **315**, 99–113.

Ferjani, I., Fattoum, A., Manai, M., Benyamin, Y., Roustan, C. and Maciver, S. K. (2010). Two distinct regions of calponin share common binding sites on actin resulting in different modes of calponin–actin interaction. *Biochimica et Biophysica Acta (BBA) - Proteins and Proteomics* **1804**, 1760–1767.

Frey, J. (1968). Die Entwicklungsleistungen der Medusenknospen und Medusen von *Podocoryne carnea* M. Sars nach Isolation und Dissoziation. *Wilhelm Roux Arch Entwickl Mech Org* **160**, 428–464.

Gabella, G. (1984). Structural apparatus for force transmission in smooth muscles. *Physiol Rev* **64**, 455–477.

Gabella, G. and Clarke, E. (1983). Embryonic development of the smooth and striated musculatures of the chicken iris. *Cell Tissue Res* **229**, 37–59.

Gold, D. A. and Jacobs, D. K. (2013). Stem cell dynamics in Cnidaria: are there unifying principles? *Dev Genes Evol* **223**, 53–66.

Gorczyca, W., Traganos, F., Jesionowska, H. and Darzynkiewicz, Z. (1993). Presence of DNA strand breaks and increased sensitivity of DNA in situ to denaturation in abnormal human sperm cells: analogy to apoptosis of somatic cells. *Exp Cell Res* **207**, 202–205.

Hao, Y., Stuart, T., Kowalski, M., Choudhary, S., Hoffman, P., Hartman, A., Srivastava, A., Molla, G., Madad, S., Fernandez-Granda, C., et al. (2022). Dictionary learning for integrative, multimodal, and scalable single-cell analysis. *bioRxiv* 2022.02.24.481684.

Haycraft, J. B. (1890). Voluntary and Reflex Muscular Contraction. *J Physiol* **11**, 352–400.

Helm, R. R., Tiozzo, S., Lilley, M. K. S., Lombard, F. and Dunn, C. W. (2015). Comparative muscle development of scyphozoan jellyfish with simple and complex life cycles. *Evodevo* **6**, 11.

Houliston, E., Momose, T. and Manuel, M. (2010). *Clytia hemisphaerica*: a jellyfish cousin joins the laboratory. *Trends in Genetics* **26**, 159–167.

Houliston, E., Leclère, L., Munro, C., Copley, R. R. and Momose, T. (2022). Past, present, and future of *Clytia hemisphaerica* as a laboratory jellyfish. In *Current Topics in Developmental Biology* (eds. Goldstein, B. and Srivastava, M.), pp. 121–151. Academic Press: Oxford.

Hsieh, T.-B. and Jin, J.-P. (2023). Evolution and function of calponin and transgelin. *Front Cell Dev Biol* **11**, 1206147.

Khaitlina, S., Fitz, H. and Hinssen, H. (2013). The interaction of gelsolin with tropomyosin modulates actin dynamics. *FEBS Journal* **280**, 4600–4611.

Koressaar, T. and Remm, M. (2007). Enhancements and modifications of primer design program Primer3. *Bioinformatics* **23**, 1289–1291.

Koressaar, T., Lepamets, M., Kaplinski, L., Raime, K., Andreson, R. and Remm, M. (2018). Primer3_masker: integrating masking of template sequence with primer design software. *Bioinformatics* **34**, 1937–1938.

Kraus, J. E. M. (2013). A comparative molecular approach on striated muscle and medusa life stage evolution in cnidarians. *PhD Thesis*. University of Vienna: Vienna.

Kraus, J. E. M., Fredman, D., Wang, W., Khalturin, K. and Technau, U. (2015). Adoption of conserved developmental genes in development and origin of the medusa body plan. *Evodevo* **6**, 23.

Kwiatkowski, D. J., Mehl, R., Izumo, S., Nadal-Ginard, B. and Yin, H. L. (1988). Muscle is the major source of plasma gelsolin. *Journal of Biological Chemistry* **263**, 8239–8243.

Lechable, M., Jan, A., Duchene, A., Uveira, J., Weissbourd, B., Gissat, L., Collet, S., Gilletta, L., Chevalier, S., Leclère, L., et al. (2020). An improved whole life cycle culture protocol for the hydrozoan genetic model *Clytia hemisphaerica*. *Biol Open* **9**, bio051268.

Leclère, L. and Röttinger, E. (2017). Diversity of Cnidarian Muscles: Function, Anatomy, Development and Regeneration. *Front Cell Dev Biol* **4**, 157.

Leclère, L., Horin, C., Chevalier, S., Lapébie, P., Dru, P., Peron, S., Jager, M., Condamine, T., Pottin, K., Romano, S., et al. (2019). The genome of the jellyfish Clytia hemisphaerica and the evolution of the cnidarian life-cycle. *Nat Ecol Evol* **3**, 801–810.

Mackie, G. O., Mills, C. E. and Singla, C. L. (1988). Structure and function of the prehensile tentilla of *Euplokamis* (Ctenophora, Cydippida). *Zoomorphology* **107**, 319–337.

Mansfield, P. J. and Neumann, D. A. (2019). Structure and Function of Skeletal Muscle. In *Essentials of Kinesiology for the Physical Therapist Assistant*, pp. 34–49. Mosby: St. Louis.

Masuda-Ozawa, T., Fujita, S., Nakamura, R., Watanabe, H., Kuranaga, E. and Nakajima, Y. (2022). siRNA-mediated gene knockdown via electroporation in hydrozoan jellyfish embryos. *Sci Rep* **12**, 16049.

Momose, T. and Houliston, E. (2007). Two Oppositely Localised Frizzled RNAs as Axis Determinants in a Cnidarian Embryo. *PLoS Biol* **5**, e70.

Momose, T., De Cian, A., Shiba, K., Inaba, K., Giovannangeli, C. and Concordet, J.-P. (2018). High doses of CRISPR/Cas9 ribonucleoprotein efficiently induce gene knockout with low mosaicism in the hydrozoan *Clytia hemisphaerica* through microhomology-mediated deletion. *Sci Rep* **8**, 11734.

Musser, J. M., Schippers, K. J., Nickel, M., Mizzon, G., Kohn, A. B., Pape, C., Ronchi, P., Papadopoulos, N., Tarashansky, A. J., Hammel, J. U., et al. (2021). Profiling cellular diversity in sponges informs animal cell type and nervous system evolution. *Science (1979)* **374**, 717–723.

Paniagua, R., Royuela, M., García-Anchuelo, R. M. and Fraile, B. (1996). Ultrastructure of invertebrate muscle cell types. *Histol Histopathol* **11**, 181–201.

Peron, S., Houliston, E. and Leclère, L. (2021). The marine jellyfish model *Clytia hemisphaerica*. In *Handbook of Marine Model Organisms in Experimental Biology: Established and Emerging Marine Model Organisms in Experimental Biology* (eds. Boutet, A. and Schierwater, B.), pp. 129–147. CRC Press.

Quiroga Artigas, G., Lapébie, P., Leclère, L., Takeda, N., Deguchi, R., Jékely, G., Momose, T. and Houliston, E. (2018). A gonad-expressed opsin mediates light-induced spawning in the jellyfish *Clytia*. *Elife* **7**, e29555.

Quiroga Artigas, G., Lapébie, P., Leclère, L., Bauknecht, P., Uveira, J., Chevalier, S., Jékely, G., Momose, T. and Houliston, E. (2020). A G protein–coupled receptor mediates neuropeptide-induced oocyte maturation in the jellyfish *Clytia*. *PLoS Biol* **18**, e3000614.

R Core Team (2022). R: A language and environment for statistical computing.

Royuela, M., García-Anchuelo, R., De Miguel, M. P., Arenas, M. I., Fraile, B. and Paniagua, R. (1996). Immunocytochemical electron microscopic study and western blot analysis of troponin in striated muscle of the fruit fly Drosophila melanogaster and in several muscle cell types of the earthworm Eisenia foetida. *Anat Rec* **244**, 148–154.

Sandow, A. (1952). Excitation-contraction coupling in muscular response. *Yale J Biol Med* **25**, 176–201.

Schindelin, J., Arganda-Carreras, I., Frise, E., Kaynig, V., Longair, M., Pietzsch, T., Preibisch, S., Rueden, C., Saalfeld, S., Schmid, B., et al. (2012). Fiji: an open-source platform for biological-image analysis. *Nat Methods* **9**, 676–682.

Schmid, B., Schmid, V. and Tardent, P. (1974). The umbrellar growth process in the leptomedusae *Phialidium hemisphaericum* (Syn. *Campanularia johnstoni*). *Experientia* **30**, 1399–1400.

Schmidt-Rhaesa, A. (2007). *The Evolution of Organ Systems*. Oxford University Press: Oxford.

Schneider, C. A., Rasband, W. S. and Eliceiri, K. W. (2012). NIH Image to ImageJ: 25 years of image analysis. *Nat Methods* **9**, 671–675.

Schultz, D. T., Haddock, S. H. D., Bredeson, J. V., Green, R. E., Simakov, O. and Rokhsar, D. S. (2023). Ancient gene linkages support ctenophores as sister to other animals. *Nature* **618**, 110.

Seipel, K. and Schmid, V. (2005). Evolution of striated muscle: Jellyfish and the origin of triploblasty. *Dev Biol* **282**, 14–26.

Seipel, K. and Schmid, V. (2006). Mesodermal anatomies in cnidarian polyps and medusae. *Int J Dev Biol* **50**, 589–599.

Shao, T. Q., Hu, B., Shao, Y., Zhang, Y. N., Liu, Y. H., Qin, J. C., Xu, Y., Fan, M. M., Duan, B. C. and Zhang, H. Q. (2020). Intraspecific variation of radial symmetry number of a 535 million-year-old jellyfish. *Precambrian Res* **349**, 105412.

Sinigaglia, C., Thiel, D., Hejnol, A., Houliston, E. and Leclère, L. (2018). A safer, urea-based in situ hybridization method improves detection of gene expression in diverse animal species. *Dev Biol* **434**, 15–23.

Sinigaglia, C., Peron, S., Eichelbrenner, J., Chevalier, S., Steger, J., Barreau, C., Houliston, E. and Leclère, L. (2020). Pattern regulation in a regenerating jellyfish. *Elife* **9**, 1–33.

Steinmetz, P. R. H., Kraus, J. E. M., Larroux, C., Hammel, J. U., Amon-Hassenzahl, A., Houliston, E., Wörheide, G., Nickel, M., Degnan, B. M. and Technau, U. (2012). Independent evolution of striated muscles in cnidarians and bilaterians. *Nature* **487**, 231–234.

Untergasser, A., Cutcutache, I., Koressaar, T., Ye, J., Faircloth, B. C., Remm, M. and Rozen, S. G. (2012). Primer3—new capabilities and interfaces. *Nucleic Acids Res* **40**, e115–e115.

Weissbourd, B., Momose, T., Nair, A., Kennedy, A., Hunt, B. and Anderson, D. J. (2021). A genetically tractable jellyfish model for systems and evolutionary neuroscience. *Cell* **184**, 5854-5868.e20.

Wickham, H., François, R., Henry, L., Müller, K. and Vaughan, D. (2023). dplyr: A Grammar of Data Manipulation.

Xu, K., Zhong, G. and Zhuang, X. (2013). Actin, spectrin, and associated proteins form a periodic cytoskeletal structure in axons. *Science* **339**, 452–6.

Supplementary Information

S1 Primer & probe sequences

Table S1: Primer sequences used for generating WMISH probes.

Gene name (BLAST)	XLOC accession number	Direction	Sequence
MTPN-like	002457	Forward	GGTAACTCCTAAACACAGCTGA
		Reverse	AGAGGAATCGTGGTCTCAGT
MLC-like	006160	Forward	ATTTAAAATGCCGCCGATGC
		Reverse	TGACTCCCTTTACAGCGTGT
stMyHC-like 1	029205	Forward	GAACAGCGCTGATTCCGAAT
		Reverse	AGATTGTAATTCGGCCGCAC
stMyHC-like 2	038183	Forward	CCGCTTGATGGCTGAATTGA
		Reverse	AAAGTGGGATCTGAGTGGGG

Table S2: Sequences of the generated WMISH probes

Gene name (BLAST)	Sequence
MTPN-like	GGCTCGAGTTTTTCAGCAAGATGGTAACTCCTAAACACA GCTGATCGCAGCAGCCATATACGCAAGTAAGCTTAAAAT AACGATATCGAGCACAAGAAAAACTCCATGAATCAACGA TGGAGACGATACCAGAAGGATTATTAGGACCTCGAAAGA AATCTAATTCGTTTAATAATCGCTTCACTGAGCAAACACG ATCTTTGACACGTTTGAACCCTGAAAGCGTATTAAAAAAA TCACCACTTCAGCGATCACAATCGACTGCTAGTATAGAGA ATGTTCTTCACAACGCTGTCTTAAGGGAAGACCATGAGGC GGTAGTTCAAATTCTGAACAATAACTTTCTTGATATAAACG CTTTCTCAATCGATGGTTTTACCTCACTTCACCAAGCTTGT ATAGTGGGTAATGAAGAGACAGTTAAGTTACTAATCGAGG CAGGGGCAGATATAACTTTGAGGACACGACGCAAGAAAT ATGAATCACCTTTAAAGTTAGCTTACCTGAACGGCAACTTC GAAGTCGCAGAATATTTGTTATCCCTTGGTGCACATGATG CGGAAATTAAAAACGGAATGTCCAAAAAATGTTTCGGAAG AGCAAACACTTTGTCTTCGTAAAATGGTTTTGAGAAACGT GTTTTTTGGGGAAGACTGCTAAATAGCCGCTGGACTTGT TTACTTTTTTTTTCGAAAAAATTGGTCCAATGGCGTTGAGTTT CAAAGCATGTTTTTCTGGATCCTTGAAAACAGTGGTATAGC CTGGAACTGAGACCACGATTCCTCTATCTTTCTAGAAGATC TCCTACAATATTCTCAGCTGCCATGGAAAATCGATGTTCTTC TTTTATTCTCTCAAGATTTTCAGGCTGTATATTAAAACTTATA TTAAGAACTATGCTAACCACCTCATCAGGAACCGTTGTAGGT GGCGTGGGTTTTCTTGGCAATCGACTCTCATGAAAACTACGA GCTAAATATTCAATATGTTCCTCTTGACCAACTTTATTCTGCA TTTTTTTTGAACGAGGTTTAGAGCAAGCTTCAGGAAACTGAG

	ACAGGAATTTTATTAAAAATTTAAATTTTGAAGAAAGTTCAGG GTTAATAGCATCCATTTTTTGCTTTGCAAGTTCCTCAGCATTC TTAACAAAAGACGTCYCTTTTGAMATGTTTAAAGTTAAACCTC CGGGGTGAAA
MLC-like	AACTTTAAACATKTCAAAAGRGACGTCTTTTGTTAAGAATGC TGAGGAACTTGCAAAGCAAAAAATGGATGCTATTAACCCTG AACTTTCTTCAAAATTTAAATTTTTAATAAAATTCCTGTCTCA GTTTCCTGAAGCTTGCTCTAAACCTCGTTCAAAAAAAATGCA GAATAAAGTTGGTCAAGAGGAACATATTGAATATTTAGCTCG TAGTTTTCATGAGAGTCGATTGCCAAGAAAACCCACGCCACC TACAACGGTTCCTGATGAGGTGGTTAGCATAGTTCTTAATATA AGTTTTAATATACAGCCTGAAAATCTTGAGAGAATAAAAGAAG AACATCGATTTTCCATGGCAGCTGAGAATATTGTAGGAGATCT TCTAGAAAGATATTTAAAATGCCGCCGATGCATGTTGACTTTG TCAAAATTTAAGCATACTCAAACTTGTGAAGGAAAGCCGTAGA GGAGAAGAAATTCCAACTTGCTAAGGAAAGTTTGGAAGAAGAG AAGAAATTGAACAGCAATGTCTCTTACTGATGATCAATTGGAG GAACTGAAAGACGCTTTCACACTTTTCGACAAGAAGGGAGAT GACAAAGTCGAGAGTGTACAAATCATCGACATTTTACGATCA CTTAAACTAAACCCGCTGACCTGCGATGTTGAAAAAGTCATC AAAGATTCCGGCTTAGAAGGCAATCGTGTCGATTTCCCAACT TTCGCTAGCATTTACGAACAATTCAAGAAACGACCTTCGATT GCAAACTATGATGACATGATTGAAATGTTCAAATGTTTTGAT CGTGAAGGAAGTAAAATGGTTTTCGGAGGTGAATTTCGAAT GGTTTTGGTCAACATGGGTGATAATATGAACCAGGAACAGAT TGAAAAAATGATCGCACCCAATGAAAATGCTGATGGGTATATC CCATACGAATCACTATTGGACTTTGTTTTGGCAAAGTAAATGA AGCACCAAAATTCCGTGCTCAAAAACCTTTAATCTGAAATGCC TAAAATAAGAGCCCTGTGGCTGAAAAATTGTAATTTATATGG AACTATGAGAATTTTCTTTGTACACGCTGTAAAGGGAGTCA ATCTTGCTGAAAAACTCGAGCCATCCCGAAG
stMyHC-like 1	GGATGGCTCGAGTTTTTCAGCAAGATAGATTGTAATTCGGC CGCGCGGTCAGCGAATTCGTTCTTCTCGTTATCGGCCAATT TGCGTGCGCGGTCAGCTTGCTCTAAGGCGACACGAGCTTCA TCGAGTTGTACAGCCAAATCGTTAGCACGTCTTTCAGATCGT GATGCAGAATCACGCATATCATCGCGACCGCGTGACTCATC ATCAATGAGGGCTTGCATCTCCTTAAGCTGGGCTTGTAATTT CTTGATAGCTTTTTGGTAGTCTCCATTCGTTCGTAAGGCACCA TCTAATTGAGATTCCAAATCAGCGACATCTGAGTCATACTTCTT CTTATTCTTCAGAAGTTCTCCCTTGGCACGTTGCTCAGCATCGA TGGTGTTTTGAAGAGAATCCATTTGTCGTTGGTGGTTCTTACGC ATCGTTTCGATTTCTTCGTCCTTTTCTGCTGAACGTCTGTCTGAC GTTTGCTTGATTTGAGTGAGCTCCAATTGGACTTTGAGATATTTG CCTTCTTCTTGTTCGAGAGCGGTTTCGGCTTCTTCCAATGCGAT TTGAAGTTCTTCATTCTCCATTCCCAACTTACGTCGAATTTTCTC CACTTCAGCTGAGCTTTTGCCTCCATCAGAAAGCTGGTCTGTGA TACTGGTGAGTTCAGCAGTCAATGCGCGGTTTTCTTTCTTGAGT GCTTCATATTTCTCTTCAGTATCTTCATGAGCAGTGCGTACTTTG AGCAATTCAGTTGAATAACCACGTGCGTCGCGTTGTGACTTGTC CAAATCCGCTTGAACCTCATCACACTTGATTTTCCATTCGTTGAT TTGTTGGTCGAATTTCTTTTGTTTCTTCTCAAGGTTGGATGCTTG TGCTTGAGCTTTCTCTAAGTCTAACAACAGGTCTTCGACTTCCT CGTTCATACGGTTCTTGACTTTCTCCATGGATGACGCTTTGGAT TCAGCAGCAGCCAAAGCTTCTTCCATCTCTTGGACTCGATTAGC CAGCTTACGTTTAGCATCTTCGAGCTCCTCAACACGGCTTGCAC CTTCCATGTCATACTTGTTCTTCCATTGGGCCGCGTCAGCGTTC

	GCGCGGGACAATTTGGCTTGGAGTTCTGAGCGSSCGGCTTGTT CCTCCTCCAGTTGTTCGTTCAAAGATTCGATY
stMyHC-like 2	CGGATGGCTCGAGTTTTTCAGCAAGATAGGTGTCGCTTTTGTT GACCGTATTGATGACCATGCTGAATATGCTGATTTACTCACCGC TGTATCTGTGTTAGGGTTCAGTGACGAAGAGAAATGGTCCATGT TCAAAATTGTTGCTTCCATCTTAAACATGGGTAACATGAAATTC AAACAAAAGCCCAGAGATGAGCAAGCTGAAGTGGTTGACCCAG CTGACGGTGAACGTGTCAGTTACTTGTTGGGAATCCCAGTCGG TGAATTCCACAAATCCCTGGTCAAACCAAAAGTCAAGGTCGGTA CCGAGTATGTCAACAAAGGACAAAATGTCAGCCAAGTCTTGTAC TCTGTCTCTGGTCTATCCAAAGCTATCTTCGAACGCATGTTCTT GTGGATTGTCCAACGTGTAAACAAGGCCTTAGACACTAAAGAA CGAAGATCTTATTTCATTGGTGTCTTGGATATCGCTGGATTCG AAATTTTCGAGTACAACTCCTTCGATCAATTGTGTATTAACTTGA CCAATGAGAAATTGCAACAATTTTTCAACCATCACATGTTCGTTC TTGAACAAGAAGAATACAAGAAAGAAGGTATCCACTGGGAATTC ATTGATTTCGGTATGGATTTGGAACAAACCATCGACTTGATCGA AAAGCCTATGGGAATTTTCGCCATGCTTGAAGAAGAATGCATCG TCCCCAAGGCTACCGATCAAACCTACTTGCAAAAATTGCACAAA CAACATGCCGGAAAGAACGCATCTTACACCAAACCAACACCCA AACAAGCCAAACAAGGTGGCGGTGATTTCATTCTCCATCATTAT GCTGGATCTGTTGGTTATTCAGTTCCCGGATGGTTGGAGAAGA ACAAGGATCCAATCAATGAAAACTCTGCTCAACTTTTCGCTAAA GCTACTGATCCATTGGTTCGTCATCTCTTCCAAGATTACAACCC AGATGTTACTGGTGGACGTAGCCGAAAGGGAAGTGCTTTCCA AACCGTCTCCTACCGTCACAAAGAGCAATTGAAGAACTTGCTCG GTACACTCATGTCAACATCCCCTCATTTCGTCCGTTATCTTTCT AGAAGATCTCCTACAATATTCTCAGCTGCCATGGAAAATCGAT GTTCTTCTTTTATTCYYYCAGGATTTTCAGGCTGTWWWTTAAAA

S2 Detailed list of chemicals, salts and buffers used

Table S3: 1X PBS composition.

Reagent	Concentration
NaCl	0.137 M
KCl	0.0027 M
Na_2HPO_4	0.01 M
KH_2PO_4	0.0018 M
H2O	Add to desired final volume
	Bring to pH 7.4

Table S4: 1X TBS composition.

Reagent	Concentration
Tris-Cl	50 mM
NaCl	150 mM

H2O	Add to desired final volume
	Bring to pH 7.6

Table S5: Tris-HCl composition.

Reagent	Concentration
Tris-base	1 M
H2O	Add to desired final volume
	Bring pH to 9.5

Table S6: 20X SSC buffer composition.

Reagent	Concentration
NaCl	3 M
Sodium citrate	0.3 M
H_2O	Add to desired final volume
	Bring to pH 7

Table S7: Hybridization buffer Hyb W composition.

Reagent	Concentration
Urea	4 M
SSC (pH 7)	5X
SDS (10%)	0.25%
Heparin	50 µg/ml
Tween20 (20%)	0.5%
Torula RNA	0.5% w/v
Dextran	1% w/v
H_2O	Add to desired final volume

Table S8: Maleic acid buffer.

Reagent	Concentration
Maleic acid	100 mM
NaCl	150 mM
	Bring to pH 7.5

Table S9: Alkaline phosphatase (AP) buffer composition.

Reagent	Concentration
NaCl	100 mM
$MgCl_2$	50 mM
Tris-HCl (pH 9.5)	100 mM
Tween 20 (20%)	0.1%
H_2O	Add to desired final volume

Table S10: Composition of the EdU detection buffer. The buffer is based on a recipe by Andrew Brumm (University of California, Los Angeles, published 2015 on ResearchGate).

Reagent	Concentration
TBS (pH 7.6)	100 mM
$CuSO_4$	4 mM
AlexaFluor 647 azide	5 µM
Ascorbic acid	100 mM

S3 Detailed WMISH protocol

If not specified otherwise, the steps are performed at room temperature. Steps at room temperature are performed in 48-well plates, steps at hybridization temperature are done in 2 ml reaction tubes.

Table S11: Rehydration of fixed animals stored in 100% MeOH.

Repetitions	Time	Reagent	Process

1x		100% EtOH	Exchange MeOH to EtOH
1x	5 min	60%/40% EtOH/0.1% PTw	Rehydrate specimens
1x	5 min	30%/70% EtOH/0.1% PTw	Rehydrate specimens
4x	5 min	0.1% PTw	Wash

Table S12: Hybridization buffer washes.

Repetitions	Time	Reagent	Process	Notes
1x	10 mins	Hyb W	Wash	
1x	1 h	Hyb W	Incubation at 57°C	
1x	5 – 10 mins	600 µl Hyb W + 12 µl probe	Denature at 70°C	During last 10 mins of Hyb W incubation
1x	ON (overnight)	Denatured probe in Hyb W	Hybridize at 57°C	Temperature should not exceed 60°C

Table S13: Post-hybridization washes.

Repetitions	Time	Reagent	Process	Notes
1x	10 mins	Hyb W	Wash at 57°C	
1x	40 mins	Hyb W	Wash at 57°C	
1x	30 mins	75% / 25% Hyb W / 0.05X SSC	Wash at 57°C	Pre-heat all reagents and perform at ON hybridization temperature
1x	30 mins	50% / 50% Hyb W / 0.05X SSC	Wash at 57°C	
1x	30 mins	25% / 75% Hyb W / 0.05X SSC	Wash at 57°C	
3x	20 mins	0.05X SSC	Wash at 57°C	

Table S14: SSC washes.

Repetitions	Time	Reagent	Process
1x	2 mins	66% / 33% 0.05X SSC / 0.1% PTw	Wash
1x	2 mins	33% / 66% 0.05X SSC / 0.1% PTw	Wash
1x	2 mins	0.1% PTw	Wash
3x	5 mins	0.5% PBT	Wash

Table S15: Probe detection.

Repetitions	Time	Reagent	Process	Notes
1x	1 h	MABR	Block specimens	In parallel
1x	1 h	1:2000 α-DIG-AB:MABR	Block AB	
1x	ON	α-DIG-AB in MABR	Incubate specimen in AB	Do in Refrigerator (4°C)

Table S16: PBT washes.

Repetitions	Time	Reagent	Process
2x	5 mins	0.2% PBT	Wash
2x	10 mins	0.2% PBT	Wash
2x	15 mins	0.2% PBT	Wash
2x	20 mins	0.2% PBT	Wash
2x	30 mins	0.2% PBT	Wash

Table S17: Specimen staining.

Repetitions	Time	Reagent	Process	Notes
3x	10 mins	AP buffer	Wash	After the last wash, leave 250 µl in the well
1x		5 µl BCIP + 5 µl NBT/ml AP buffer	Stain	Add 250 µl per well to a final volume of 500 µl per well. Leave in dark until staining is satisfactory.
1x	5 mins	1% PTw	Wash	
1x	1 h – ON	>96% EtOH	Wash	Until background is removed. If done ON, leave at 4°C.
2x	10 mins	0.1% PTw	Wash	
1x		87% Glycerol	Store	

S4 Supplementary figures and tables

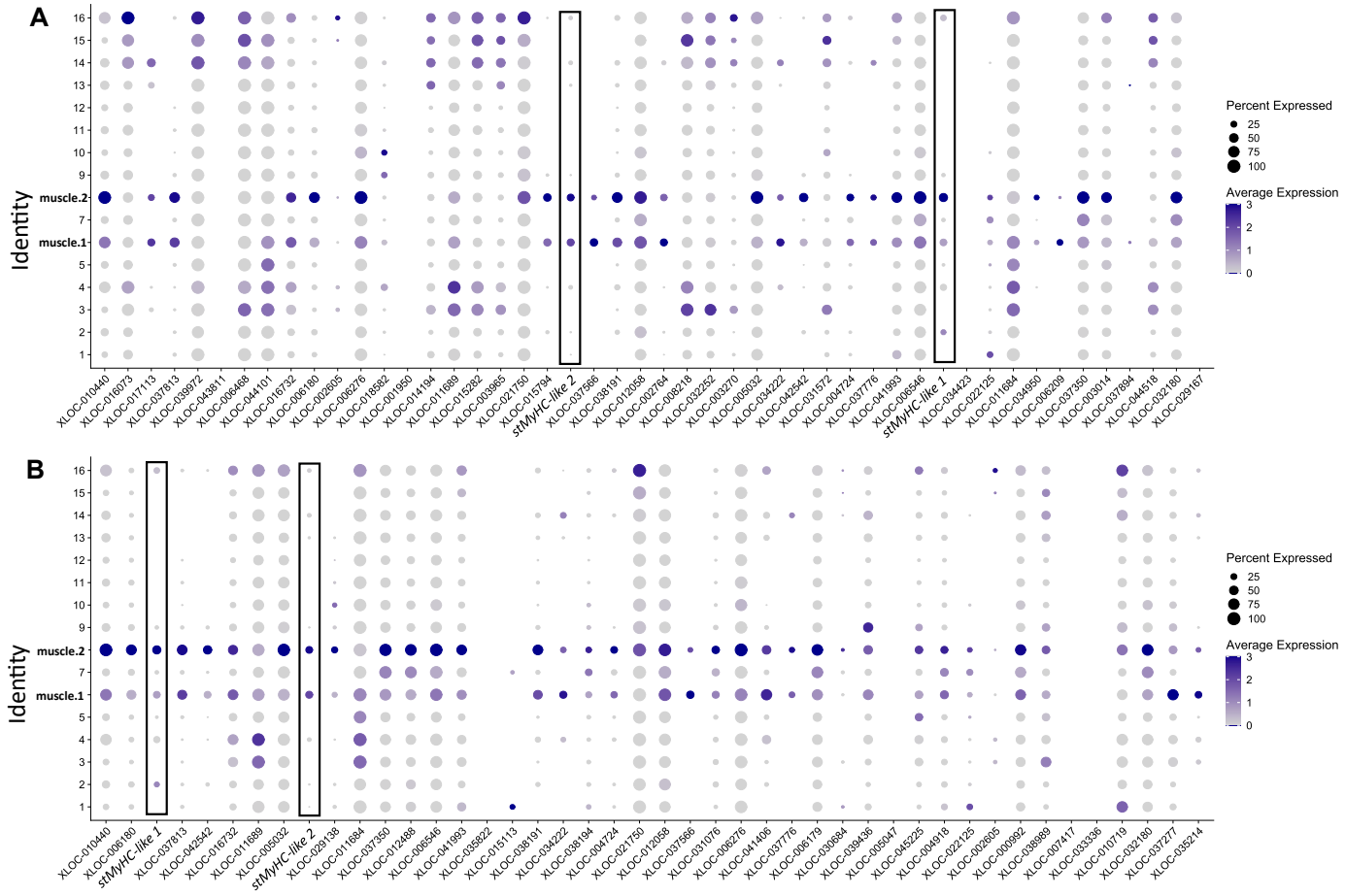

Fig. S1: Marker genes of the Chari et al. (2021) paper, plotted against the clusters identified in this study. Genes used for our study are highlighted **A**: Marker genes for the striated muscles of the velum. **B**: Marker genes for the striated muscles of the subumbrella. As visualized here, the marker genes do not show a difference between the two striated muscles clusters in our dataset, the marker genes for either cluster in the reference dataset are found in both clusters of our dataset.

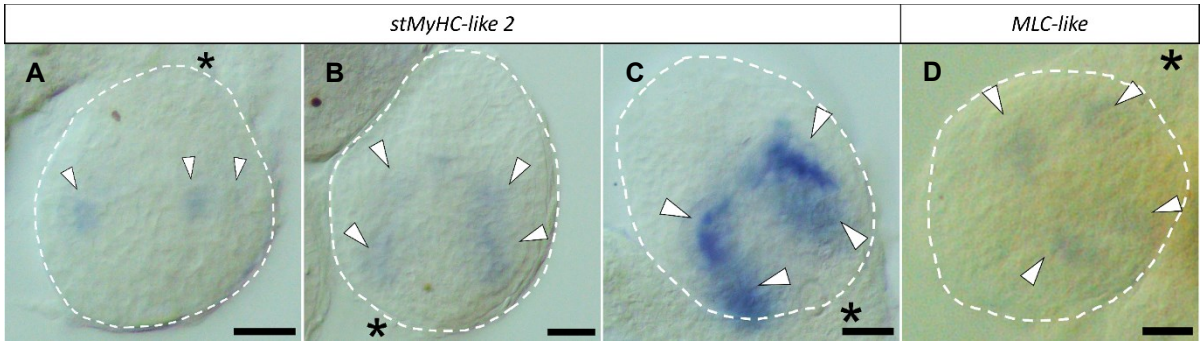

Fig. S2: Onset of striated muscle gene expression in medusa buds. All images show a lateral view of the medusa buds (white outlines). Asterisks indicate the area where the bud is attached to the stalk. White arrowheads show gene expression of *stMyHC-like 2* (**A**-**C**, increasing developmental stages) and *MLC-like* (**D**, comparable developmental stage as **A**) following the same quadruple arrangement as seen with *stMyHC-like 1* (Fig. 14A-D). Scale bars: 25 µm

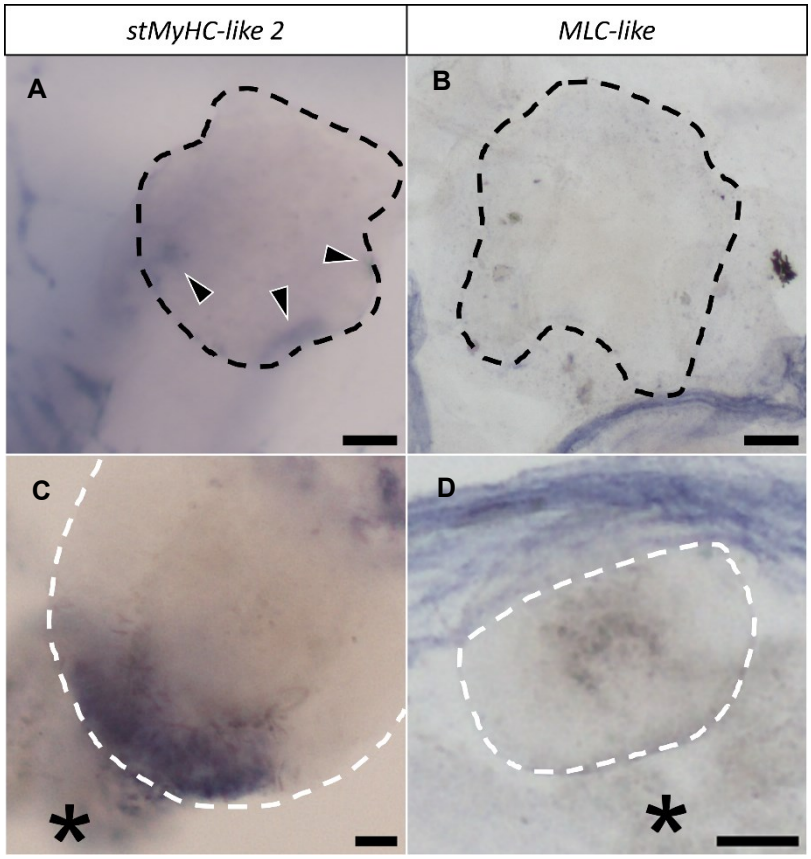

Fig. S3: Additional details of gene expression in the manubrium (**A**, **B**, black outline) and tentacle bulbs (**C**, **D**, white outline) of medusae. *stMyHC-like 2* is expressed in streaks along the proximal-distal axis of the manubrium (**A**, black arrowheads). No such expression pattern is visible in the for *MLC-like* (**B**). Note that **A** and **B** are top-down views on the manubrium tip. In tentacle bulbs, gene expression of *stMyHC-like 2* can be found in the proximal-sided half (**C**), where the tentacle emerges from the bulb (denoted by an asterisk). *MLC-like* is not expressed in the tentacle bulbs (**D**). Scale bars: 100 µm (**B**), 50 µm (**D**), 10 µm (**A**, **C**)

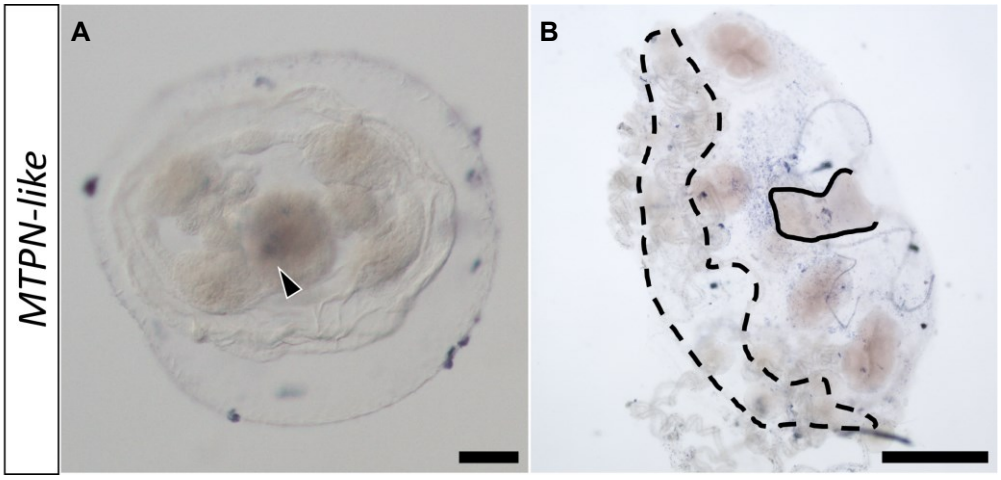

Fig. S4: Expression of *MTPN-like* in medusae. Expression of this gene can only be detected in freshly hatched medusae (**A**) at the location of the manubrium (black arrowhead). However, no more expression can be found in adult medusae (**B**). Black dotted outline in **B** shows the bell rim/velum, with the black solid line indicating the position of the manubrium. Scale bars: 50 µm (**A**), 500 µm (**B**),

Table S18: List of genes of the putative muscles clusters with their gene ontology (GO) terms specific for bilaterian sarcomere function.

Accession numbers	Putative muscle clusters	Gene descriptions (best BLAST hit)	Bilaterian sarcomere GO function
XLOC_011539	1	Myosin tail	Myosin complex
XLOC_042927	1	Myosin head; MyTH4 domain; IQ-motif; FERM domain; Pleckstrin homology domain	ATP binding; protein binding; myosin complex
XLOC_029205, XLOC_038183	1, 2	Myosin head; myosin tail; IQ-motif	ATP binding; protein binding; myosin complex
XLOC_009470	1	Spectrin alpha chain; SH3 domain; Rho GTPase activation protein; FCH domain	Protein binding
XLOC_014627	1	Gas2-related domain; Calponin homology domain	Protein binding
XLOC_032648	1	Immunoglobulin-like fold; Calponin homology domain; Filamin repeat; Actinin-type domain	Protein binding
XLOC_033234	1	FAD/NAD(P)-binding domain; Calponin homology domain; Zinc finger, LIM-type	Protein binding
XLOC_037277	1, 2	Smooth muscle protein/Calponin	Protein binding
XLOC_034950	2	Smooth muscle protein/Calponin	Protein binding
XLOC_006160, XLOC_006180, XLOC_016732, XLOC_037566	1, 2	EF-hand domain pair	Calcium ion binding
XLOC_000112, XLOC_011348	1	EF-hand domain pair	Calcium ion binding
XLOC_006671	1	EF-Hand domain pair; Small GTPase superfamily	Calcium ion binding
XLOC_009401	1	EF-hand domain pair; GRAM domain; PH domain-like	Calcium ion binding
XLOC_015114	1, 2	Actin-depolymerizing factor homology domain; ADF/Cofilin; Gelsolin-like domain	LIM protein actin filament binding

XLOC_044563	1	Villin/Gelsolin; Villin headpiece; Gelsolin-like domain; ADF-H	LIM protein actin filament binding
XLOC_000272	1	Kinesin motor domain	ATP binding
XLOC_002281, XLOC_005670, XLOC_014440	1	Protein kinase domain; Serine/Threonine-protein kinase	ATP binding
XLOC_005191	1	Heat-shock protein 70; Chaperone DnaK	ATP binding
XLOC_006929	1	Heat-shock protein Hsp90; Histidine kinase-like ATPase	ATP binding
XLOC_011535	1	ATPase, AFGf1-like	ATP binding
XLOC_012048	1	AGC-kinase; Protein kinase; cGMP-dependent kinase; Cyclic nucleotide binding; RmlC-like jelly roll fold	ATP binding
XLOC_013768	1	Mitogen-activated protein kinase; Protein kinase; Serine/threonine-protein kinase	ATP binding
XLOC_019988	1	GroEL-like domain; Chaperonin Cpn60/TCP-1	ATP binding
XLOC_036044	1	Helicase superfamily 1/2; Myb-like domain; SNF-2 related	ATP binding
XLOC_039705	1	Helicase superfamily 1/2; DEAD/DEAH helicase domain; RNA helicase	ATP binding
XLOC_040238	1	GroES chaperonin family	ATP binding
XLOC_043393, XLOC_043406	1	ABC transporter-like	ATP binding
XLOC_000117	2	Aminoacyl-tRNA synthetase; MICOS complex subunit	ATP binding
XLOC_004301	2	Protein kinase domain; Serine/threonine-kinase	ATP binding
XLOC_004376	2	Nucleoside diphosphate kinase	ATP binding
XLOC_012448	2	ATP synthase F1 complex; ATPase F1/V1/A1 complex	ATP binding
XLOC_045734	2	DEAD/DEAH box helicase domain; Helicase superfamily 1/2	ATP binding

XLOC_010440	1, 2	Protein kinase; Immunoglobulin subtype	ATP binding
XLOC_031076	1, 2	ATP-citrate lyse/succinyl-CoA ligase; ATP grasp fold	ATP binding
XLOC_037350	1, 2	ATP synthase F1 complex; ATPase F1/V1/A1 complex	ATP binding
XLOC_040993	1, 2	DNA recombination/repair protein Rad51	ATP binding

S5 GO-filtering code and GO-terms used

```
library("readxl")
library("dplyr")
data1 = read_excel("differential_annotated_gene_list.xlsx")
Unfold <- data1 %>%
      dplyr::mutate(`GOs` = strsplit(as.character(`GOs`), ",")) %>%
      tidyr::unnest(`GOs`)
filter <- Unfold %>% dplyr::filter(GOs == "Insert_GO_Number_Here")
GO_Term_Cluster <- filter %>% dplyr::filter(cluster == "Insert_Cluster_Here")
```

Table S19: List of GO-terms specific to bilaterian sarcomere assembly. Terms highlighted in bold and italic were found in our differential expressed genes.

GO-Number	Description
GO:0001952	regulation of cell matrix adhaesion
GO:0003009	skeletal muscle contraction
GO:0003779	***LIM protein Actin filament binding***
GO:0005509	***calcium ion binding***
GO:0005515	***protein binding***
GO:0005516	Calmodulin binding
GO:0005523	***Tropomyosin binding***
GO:0005524	***ATP binding***
GO:0005859	muscle myosin complex
GO:0005915	zonula adhaerens
GO:0005925	***focal adhaesion***
GO:0006936	muscle contraction
GO:0007512	adult heart development
GO:0008307	structural constituent of muscle
GO:0014820	tonic smooth muscle contraction
GO:0016459	***Myosin complex***
GO:0016461	unconventional myosin complex

GO:0016462	myosin II complex
GO:0016528	Sarcoplasm
GO:0016529	Sarcoplasmic reticulum
GO:0030018	z-disc
GO:0030047	Actin modification (phosphorylation/ubiquitination
GO:0030048	Actin filament based movement
GO:0030049	muscle filament sliding
GO:0030239	myofibril assembly
GO:0030240	skeletal muscle thin filament assembly
GO:0030241	skeletal muscle thick filament assembly
GO:0030315	T-tubule
GO:0031005	filamin binding
GO:0031032	***Actomyosin structure organization***
GO:0031430	M-band
GO:0031432	Titin binding
GO:0031672	A band
GO:0031674	I Band
GO:0031941	filamentous actin
GO:0035508	positive regulation of myosin-light-chain-phosphatase activity
GO:0042383	Sarcolemma
GO:0042642	actomyosin
GO:0042805	Actinin binding
GO:0045159	myosin II binding
GO:0045214	sarcomere organization
GO:0048769	sacromerogenesis
GO:0051014	Actin filament severing/barbed end actin capping
GO:0051015	***Actin filament binding/ Actin crosslinking activity***
GO:0051016	barbed end Actin filament capping activity
GO:0051371	Muscle alpha actinin binding
GO:0051373	FATZ binding
GO:0051694	***pointed-end actin filament capping***
GO:0055001	muscle cell development
GO:0055003	cardiac myofibril assembly
GO:0055008	cardiac muscle tissue morphogenesis
GO:0060048	cardiac muscle contraction
GO:0061061	muscle structure development
GO:0070080	titin z domain binding
GO:0071691	cardiac muscle thin filament assembly
GO:1990733	Titin-Telethonin complex